

REVIEW SUMMARY

NANOMATERIALS

Semiconductor quantum dots: Technological progress and future challenges

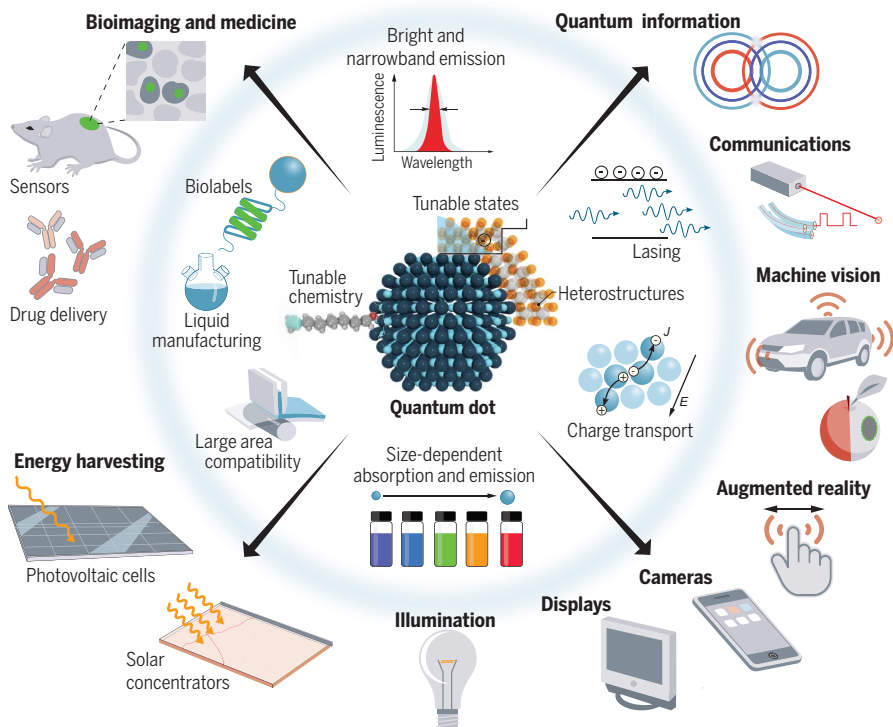
F. Pelayo García de Arquer, Dmitri V. Talapin, Victor I. Klimov, Yasuhiko Arakawa, Manfred Bayer, Edward H. Sargent*

BACKGROUND: Semiconductor materials feature optical and electronic properties that can be engineered through their composition and crystal structure. The use of semiconductors such as silicon gallium arsenide sparked technologies from computers and mobile phones to lasers and satellites. Semiconductor quantum dots (QDs) offer an additional lever: Because their size is reduced to the nanometer scale in all three dimensions, the restricted electron motion leads to a discrete atom-like electronic structure and size-dependent energy levels. This enables the design of nanomaterials with widely tunable light absorption, bright emission of pure colors, control over electronic transport, and a wide tuning of chemical and physical functions because of their large surface-to-volume ratio.

ADVANCES: The bright and narrowband light emission of semiconductor QDs, tunable across the visible and near-infrared spectrum, is attractive to realize more efficient displays with purer colors. QDs are engineered compositionally and structurally to manipulate energy states and charge interactions, leading to optical gain and lasing, relevant to light emission across visible and infrared wavelengths and fiberoptic communication. Their tunable surface chemistry allows application as optical labels in bio-imaging, made possible by tethering QDs with proteins and antibodies. The manipulation of QD surfaces with capping molecules that have different chemical and physical functions can be tailored to program their assembly into semiconducting solids,

increasing conductivity and enabling the transduction of photonic and chemical stimuli into electrical signals. Optoelectronic devices such as transistors and photodetectors lead to cameras sensitive to visible and infrared light. Highly crystalline QDs can be grown epitaxially on judiciously chosen substrates by using high-temperature and vacuum conditions, and their use has led to commercially viable high-performance lasers. The advent of colloidal QDs, which can be fabricated and processed in solution at mild conditions, enabled large-area manufacturing and widened the scope of QD application to markets such as consumer electronics and photovoltaics.

OUTLOOK: From a chemistry perspective, further advances in QD fabrication are needed to sustain and improve desired chemical and optoelectronic properties and to do so with high reproducibility. This entails the use of inexpensive synthesis methods and precursors that are able to retain laboratory-scale QD properties to market-relevant volumes. A better understanding of the yet-incomplete picture of QD surfaces, atomic arrangement, and metastable character is needed to drive further progress. From a regulatory perspective, added attention is needed to achieve high-quality materials that do not rely on heavy metals such as Cd, Pb, and Hg. The role of nanostructuring in toxicity and life cycle analysis for each application is increasingly important. From a materials and photophysics perspective, exciting opportunities remain in the understanding and harnessing of electrons in highly confined materials, bridging the gap between mature epitaxial QDs and still-up-and-coming colloidal QDs. The yet-imperfect quality of the latter—a price paid today in exchange for their ease of manufacture—remains a central challenge and must be addressed to achieve further increased performance in devices. From a device perspective, colloidal QD manufacturing must advance to translate from laboratory-scale to large-area applications such as roll-to-roll and inkjet printing. Photocatalysis, in which light is used to drive chemical transformations, is an emerging field in which QDs are of interest. Quantum information technologies, which rely on the transduction of coherent light and electrons, bring new challenges and opportunities to exploit quantum confinement effects. Moving forward, opportunities remain in the design of QD-enabled new device architectures. ■



Semiconductor quantum dot technologies. QDs feature widely tunable optical, electrical, chemical, and physical properties. Their applications span energy harvesting, illumination, displays, cameras, sensors, communication and information technology, biology, and medicine. These nanostructures have been exploited to realize efficient lasers, displays, biotags, and solar harvesting devices available in the market and are emerging in photovoltaics, sensing, and quantum information.

The list of author affiliations is available in the full article online.

*Corresponding author. Email: ted.sargent@utoronto.ca

Cite this article as F. P. García de Arquer et al., *Science* **373**, eaaz8541 (2021). DOI: 10.1126/science.aaz8541

S READ THE FULL ARTICLE AT
<https://doi.org/10.1126/science.aaz8541>

REVIEW

NANOMATERIALS

Semiconductor quantum dots: Technological progress and future challenges

F. Pelayo García de Arquer^{1,2}, Dmitri V. Talapin³, Victor I. Klimov⁴, Yasuhiko Arakawa⁵, Manfred Bayer⁶, Edward H. Sargent^{1*}

In quantum-confined semiconductor nanostructures, electrons exhibit distinctive behavior compared with that in bulk solids. This enables the design of materials with tunable chemical, physical, electrical, and optical properties. Zero-dimensional semiconductor quantum dots (QDs) offer strong light absorption and bright narrowband emission across the visible and infrared wavelengths and have been engineered to exhibit optical gain and lasing. These properties are of interest for imaging, solar energy harvesting, displays, and communications. Here, we offer an overview of advances in the synthesis and understanding of QD nanomaterials, with a focus on colloidal QDs, and discuss their prospects in technologies such as displays and lighting, lasers, sensing, electronics, solar energy conversion, photocatalysis, and quantum information.

The electronic and optical properties of conventional bulk semiconductors are determined by materials composition, crystal structure, and intentional and unintentional impurities (dopants). Advances in layer-by-layer crystal growth techniques such as molecular beam epitaxy (MBE) and metal organic chemical vapor deposition (MOCVD) enabled the realization of highly crystalline Si and III-V (for example, GaAs, InP, and GaN) semiconductors (1) with widely tunable optoelectronic properties. Quantum-confined structures exhibit size-dependent electronic properties, leading to extra degrees of tunability compared with bulk semiconductors and additional levers in the design of materials and devices.

Quantum confinement emerges when electrons are constrained to a domain comparable with their de Broglie wavelength. Quantum-confined structures are classified as two-dimensional (2D)—in which electrons are free to move in two directions—1D, and 0D. These include quantum wells, quantum wires, and quantum dots (QDs), respectively. In QDs, electrons and holes exhibit a discrete (quantized), atomic-like density of states (DOS) (Fig. 1A) (2). As QDs become smaller, quantum confinement increases the effective bandgap, leading to a blue shift of the absorption and emission spectra. An electron excited across the bandgap

experiences strong interactions with the remaining valence band hole. Coulomb attraction and spin-exchange coupling produce strongly confined electron-hole pairs (excitons). Under high excitation levels, multiple excitons populate a QD. The close proximity between charge carriers in QDs leads to enhanced many-body phenomena that affect their electronic and optoelectronic properties (3).

QDs were first realized experimentally as glass-embedded particles (Fig. 1B) (4) and, shortly after that, as chemically synthesized colloidal nanocrystals (5, 6). Independently, the concept of 3D quantum confinement in semiconductor nanostructures for lasing applications was presented (7) and demonstrated by combining a quantum well potential with high magnetic fields (8). The resulting structures were labeled 3D quantum wells or quantum well boxes.

Fabrication and assembly of QDs

Two main strategies exist to fabricate QDs: physical vacuum-based methods and wet-chemical approaches.

Top-down physical fabrication relies on lithography or milling to define a nanometer-sized volume in an existing semiconductor (Fig. 1C). In bottom-up techniques, QD growth occurs through assembly of atomic or molecular building blocks and is driven by built-in strain [Stranski-Krastanov (S-K) growth mode]. MBE and MOCVD have enabled the realization of high-quality epitaxial QDs (eQDs) prepared on top of a crystalline substrate (Fig. 1D). S-K growth was used to achieve In(Ga)As/GaAs eQDs (9–11). Alternative droplet epitaxial growth of eQDs occurs through sequential deposition of group III and V atoms without using lattice-mismatch, offering a path toward strain-free eQDs that is yet to be fulfilled (12). eQDs have

been applied in areas such as optical fiber communications (as laser sources), military night-vision cameras, and aerospace (for example, optoelectronic circuits and ultrahigh-efficiency solar cells) (13).

The chemical solution-phase fabrication of colloidal QDs (cQDs) is an approach distinct to physical vacuum-based epitaxy. Modern cQD syntheses can be traced to the colloidal method introduced in 1993 (14). The synthetic methodology for cQDs evolved from early work on arrested precipitation of inside small aqueous micelles (15) toward reactions between molecular precursors in organic solvents at mild temperatures (100° to 350°C) (Fig. 1E). The nucleation and growth of cQDs is controlled by surfactant molecules (ligands) that bind dynamically to cQD surfaces. Judicious selection of precursors and surfactants, as well as manipulation of reaction temperature and duration, enable precise control over the stoichiometry, size, and shape of the cQD. Colloidal approaches have been successfully applied to grow cQDs of II-VI (14), III-V (16), IV-VI (17), and group IV (18–20) semiconductors and, more recently, metal halide perovskites (CsPbX₃; X = I, Br, or Cl) (21).

The quality of cQDs is determined by the crystalline perfection of their cores, the completeness of surface passivation, and uniformity in size and shape. High monodispersity is crucial to retaining the near-discrete character of the DOS for an ensemble of cQDs. Exploration of the ample synthetic parameter space has led to a continued improvement in cQD syntheses, leading to absorption linewidths approaching the homogeneous (single QD) limit (14, 22, 23). Doping of cQDs provides an additional avenue to tune their DOS and type of majority charge carrier (24–26).

The surface ligands in cQDs—typically bulky organic molecules, such as oleic acid and oleylamine—introduce repulsive forces between cQDs dispersed in a solvent, rendering them colloidally stable (27). The deposition of cQDs onto solid substrates can lead to either glassy or partially ordered QD films, determined by nanocrystal monodispersity, solvent drying kinetics, and the interaction among surface ligands (28–32).

Solution-based cQD deposition techniques are scalable and well-suited for the realization of large-area devices. cQD thin-film fabrication is compatible with high-throughput manufacturing and with a variety of substrates, which facilitates integration with platforms such as silicon electronics, plastic circuits, fiber optics, and fabrics.

QDs: From engineered functionalities to applications

Size-dependent bandgap

The bandgap of QDs (E_g) can be size-tuned across a wide range of energies from the

¹Department of Electrical and Computer Engineering, University of Toronto, 35 St. George Street, Toronto, ON M5S 1A4, Canada. ²CFO-Institut de Ciències Fotòniques, The Barcelona Institute of Science and Technology, Barcelona 08860, Spain. ³Department of Chemistry, University of Chicago, Chicago, IL 60637, USA. ⁴Chemistry Division, C-PCS, Los Alamos National Laboratory, Los Alamos, NM 87545, USA. ⁵University of Tokyo, Meguro, Tokyo 153-8505, Japan. ⁶Technische Universität Dortmund, 44221 Dortmund, Germany.
*Corresponding author. Email: ted.sargent@utoronto.ca

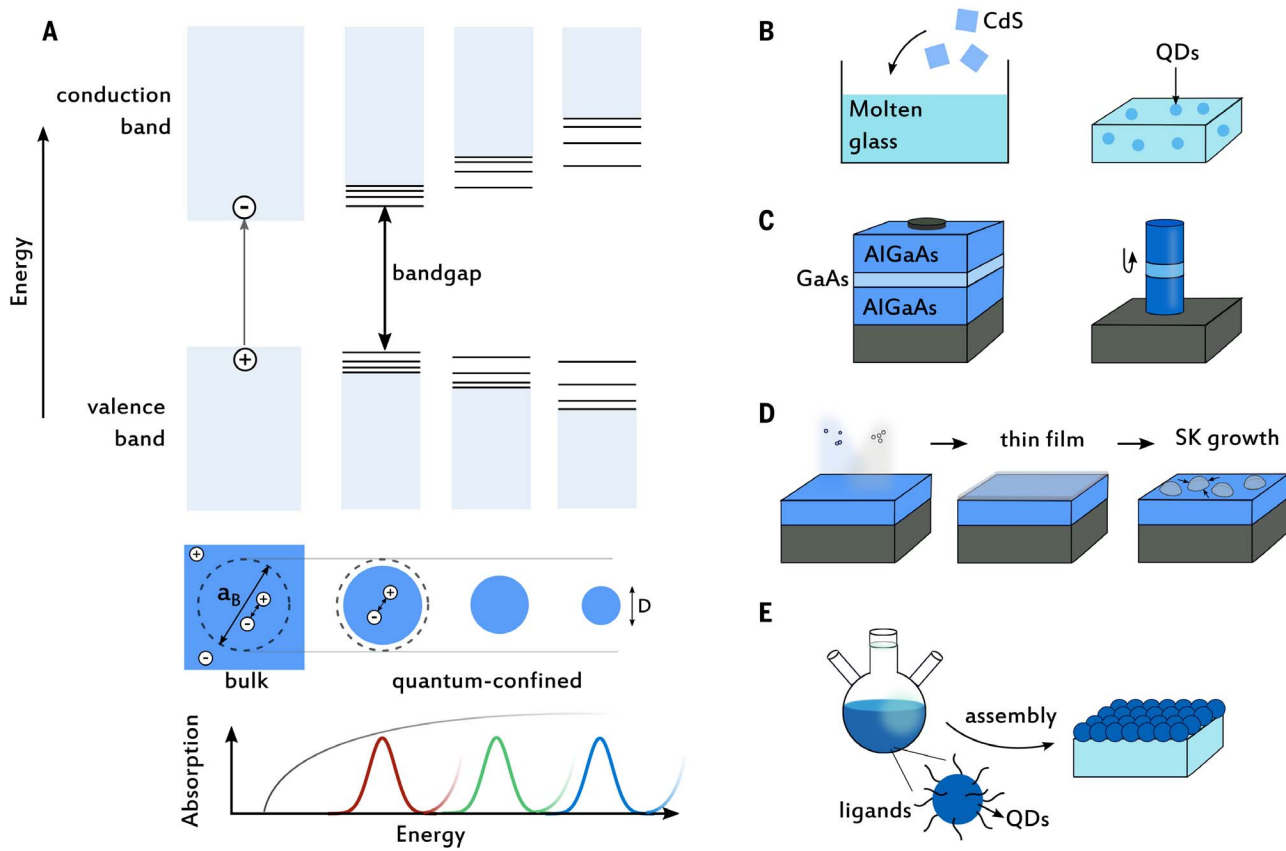


Fig. 1. Quantum confinement and fabrication of QD materials. (A) Quantum confinement, leading to size-dependent optical and electrical properties that are distinct from those of parental bulk solids, occurs when the spatial extent of electronic wave functions is smaller than the Bohr exciton diameter (a_B). D , QD diameter. (B to E) Examples of OD semiconductor

nanostructures, including early demonstrations of high-temperature precipitation in molten glasses; top-down lithography; nucleation and growth of nano-islands through epitaxial layer-by-layer deposition by using molecular beam epitaxy (MBE); and solution-based, low-to-moderate temperature colloidal synthesis.

ultraviolet (UV) to the infrared (IR) (Fig. 1A). The lower-bound on E_g is set by the bandgap of the parental bulk solid. Control over E_g is central to QD-based technologies, affecting solar energy harvesting, lighting and displays, lasers for telecommunications, sensing, metrology, imaging, and medical diagnostics.

Narrow linewidth, bright emission

In highly monodisperse cQD samples, the discrete, atomic-like structure of electronic states leads to a narrow ensemble emission linewidth of 20 to 80 meV at room temperature [defined as a full width at half maximum (FWHM)], which approaches a single-dot linewidth (23, 33). This enables the high color purity needed to reach target performance in next-generation displays (34). Best cQD samples also achieve near-unity photoluminescence quantum yield (PLQY; the number of emitted photons per absorbed photon) (35). The narrowband and bright emission of the cQDs has been exploited in commercial televisions and displays. These features are also of interest for luminescent solar concentrators (LSCs), devi-

ces that act as large-area sunlight collectors for PV modules (36).

In lasing, the discrete character of QD electronic states is an important advantage. The sharp DOS concentrates oscillator strength into the desired ground-state transition, while a wide separation between quantized energy levels inhibits thermal depopulation of the emitting band-edge states (7). Present-day commercial QD lasers are realized by using S-K grown In(Ga)As/GaAs eQDs. cQD-based lasers are still under active development (37).

Tunable surface chemistry

QDs feature a large surface-to-volume ratio, making them sensitive to their environment. In cQDs, the surfaces are typically terminated with molecules or ions with different morphologies and functional groups (27, 38). This offers a route to manipulate cQD interactions with their environment. cQDs can be tethered to proteins, antibodies, or other biologic species and used as optically addressable biolabels (39).

“Surface programming” offers an additional tool for manipulating energy levels and driv-

ing the assembly of cQDs into conductive semiconductor solids. Ligand exchange strategies seek to replace bulky molecules with shorter, more conductive ligands to enhance interdot coupling and facilitate charge transport (27, 40). This process can be carried out while the cQDs are in a liquid solution or after they had been assembled into a solid film. It is necessary that these steps do not distort electronic surface passivation so as to prevent formation of intra-gap states that would compromise electronic and optical properties (41).

Tunable charge transport

The ability of cQD assemblies to pass current is determined by the ability of charge carriers to cross interparticle barriers (42). cQD solids exhibit modest charge carrier mobilities (typically below $10^{-1} \text{ cm}^2 \text{ V}^{-1} \text{ s}^{-1}$) compared with Si or epitaxial III-Vs semiconductors (10^2 to $10^3 \text{ cm}^2 \text{ V}^{-1} \text{ s}^{-1}$). Most cQD solids exhibit a complex interplay between carrier confinement, cQD interfacial properties, and electronic coupling. Enhanced cQD coupling for higher mobility is often accompanied by the increase

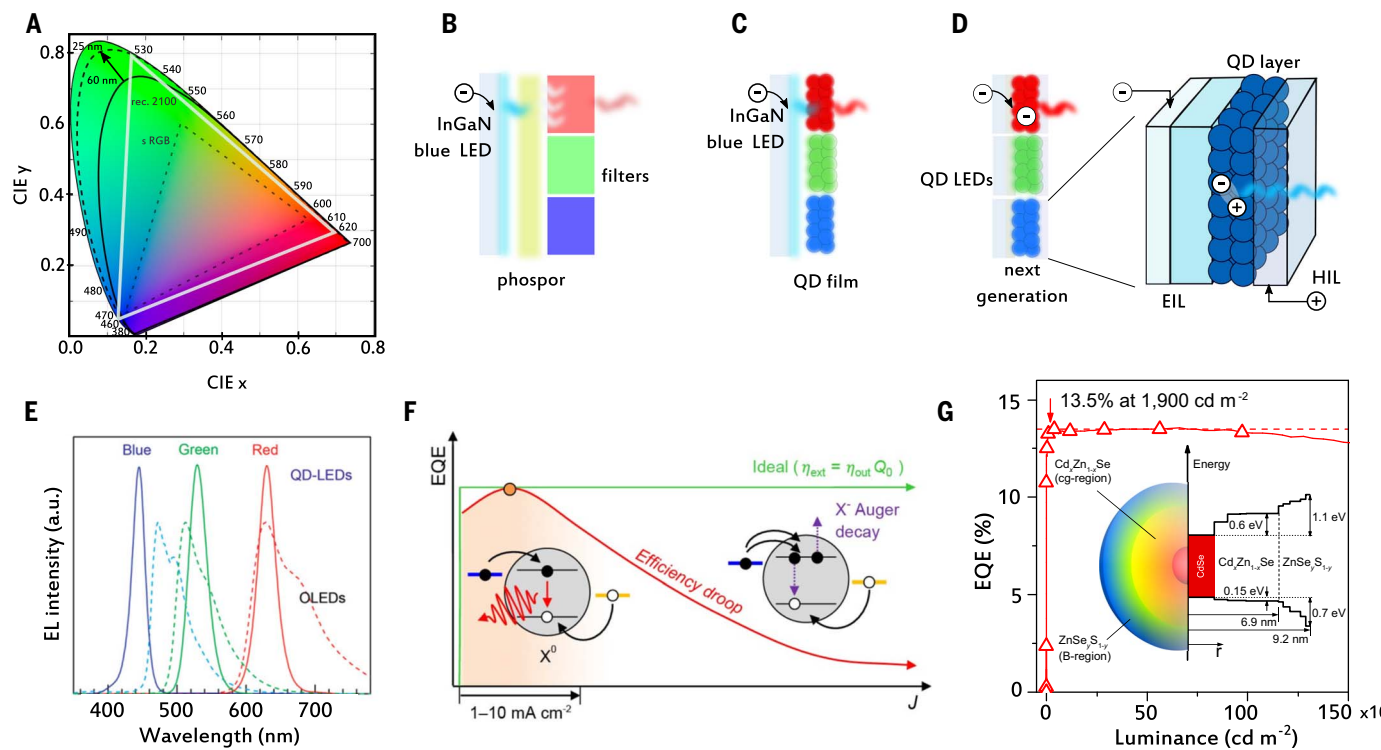


Fig. 2. QD materials for displays and lighting. (A) In displays, red, green, and blue colors are mixed to obtain entire color palette. Chromaticity diagrams are used to quantify the quality of color for displays. The triangles represent the color gamut standard for current (sRGB) and next-generation displays (Rec. 2100) (34). (B) to (D) Different QD-enabled display technologies in which QDs are excited either optically or electrically. EIL and HIL are electron and hole injection layers, respectively. (E) Illustration of high color purity of QD emission (solid lines) compared

with those of OLEDs emitting at similar wavelengths (dashed lines) (48). (F) Efficiency droop in QD-LEDs. EQE roll-off at higher current densities (J) is typically a result of imbalanced electron and hole injections, which leads to accumulation of long-lived uncompensated charges and associated carrier losses due to nonradiative Auger recombination. (G) A virtually droop-free EQE of ~13.5% maintained up to high luminance levels of $\sim 0.15 \text{ Mcd m}^{-2}$ is realized by using cQDs with suppressed Auger recombination, achieved by grading the cQD composition (inset) (52).

of intra-gap tail states that shrink the electronic gap of the cQD solid. The passivating layers, added to preclude cQD fusion and suppress intra-gap states, often introduce charge-transport barriers between adjacent dots. By controlling these competing trends, mobilities up to $10 \text{ cm}^2 \text{ V}^{-1} \text{ s}^{-1}$ for one type of carrier have been realized (43, 44). Recently, encouraging progress has been achieved for cQD solids showing balanced charge transport for both polarities (n and p) that preserve discrete quantum-confined electronic states (45).

QD technologies and challenges

QD materials for displays and lighting

The narrowband cQD emission represents a competitive advantage compared with other semiconductors for the generation of pure colors, a requisite for next-generation displays (Fig. 2A). Displays can use cQDs either as color-converting phosphors excited by light-emitting diodes (LEDs) or as active electroluminescent materials directly driven by an applied bias. In the first mode (Fig. 2B), a polymer composite containing red- and green-emitting nanocrystals is combined with a backlight unit frame of blue InGaN LEDs, incorporated into a liquid-

crystal display architecture as an RGB (red-green-blue) backlight (46). This approach offers improved color gamut and reduced light losses during color filtering as compared with those of traditional white LED backlight approaches. In another scheme, patterned cQDs are used as a photoactive material, absorbing short-wavelength blue light and re-emitting light of longer-wavelength blue, green, and red colors (Fig. 2C). This eliminates the need for separate color filters, removing color cross-talk (47); reduces the number of layers in the device stack; enhances the viewing angle; and increases the light output and device efficiency.

In cQD-based electroluminescent structures, cQDs are used to implement RGB LEDs that are addressed electrically (Fig. 2D). This approach can help reduce screen thickness, enhance dynamic range, improve black-color rendering, and increase viewing angle and frame rates. Compared with organic LEDs (OLEDs), cQD-based LEDs offer narrower emission linewidths (<30 nm versus >60 nm for OLEDs) (Fig. 2E) and correspondingly higher color purity, as needed to meet Rec. 2100 color gamut specifications (34, 48).

In QD-LEDs, a cQD active layer is sandwiched between electron and hole injecting

layers (Fig. 2D). An important LED characteristic is the external quantum efficiency (EQE)—the ratio of the number of emitted photons to the number of injected electrons. The prerequisites of high EQEs are a high PLQY and good balance between electron and hole injection currents to avoid CQD charging because the formation of charged excitons promotes nonradiative Auger recombination (49, 50). During Auger decay, the electron-hole recombination energy is released not as a photon but instead transferred to the resident charge carrier (Fig. 2F). Auger recombination has been identified as at least one of the reasons for EQE droop—a decrease in device efficiency with increasing current density. This creates problems even in the case of standard displays operating at low-to-moderate brightness (500 to 1000 cd m^{-2}); and becomes a serious challenge for outdoor systems whose brightness should be comparable with or greater than that of natural sunlight (5000 cd m^{-2}).

The droop problem has been tackled with both device optimization and cQD structure control. Compositionally graded cQD multishell heterostructures have been shown to impede Auger recombination because of creation of a “smooth” confinement potential that suppresses

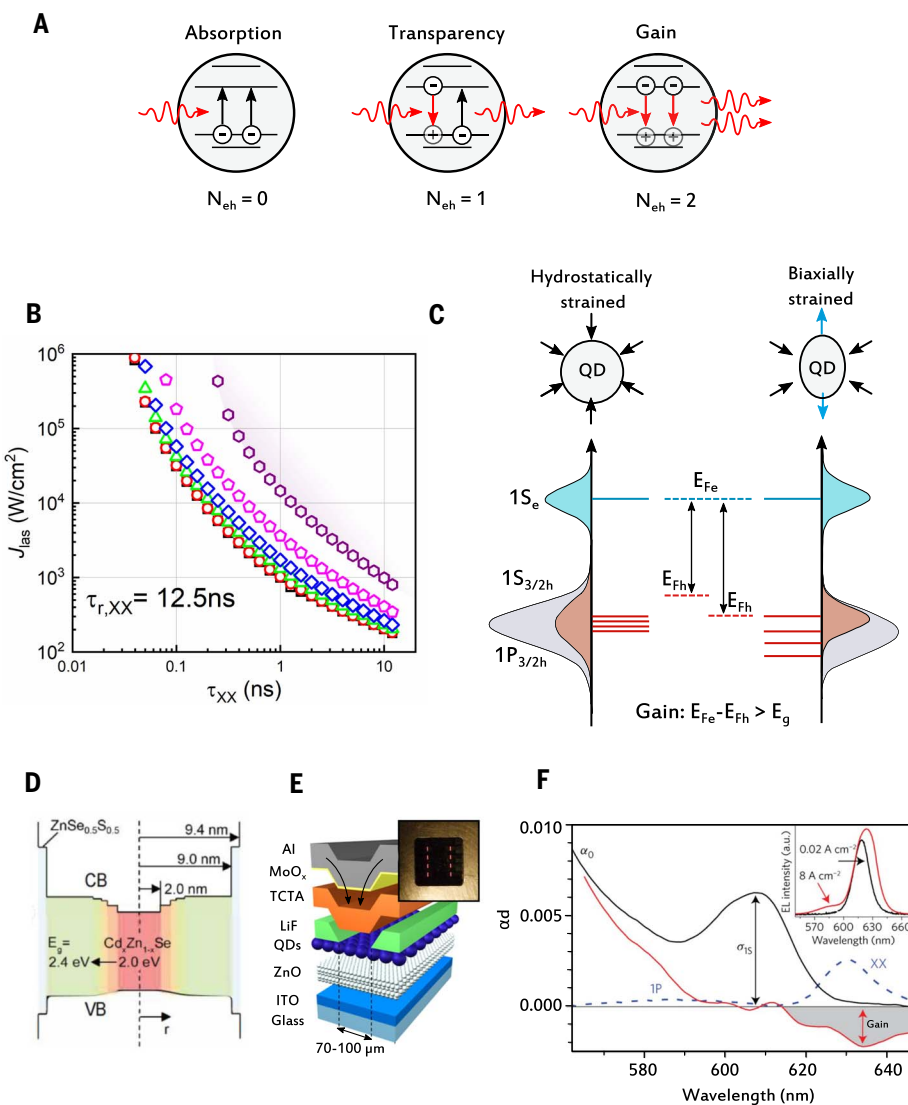


Fig. 3. Principles of QD lasing and recent advances. (A) Optical gain in QDs originates from biexcitons; hence, suppression of Auger recombination is critical to realize lasing, especially in the case of cw optical and dc electrical pumping (63). (B) Modeling indicates strong dependence of the cw lasing threshold on biexciton lifetime ($\tau_{r,XX} = \tau_{r,XX}\tau_{A,XX}/(\tau_{r,XX} + \tau_{A,XX})$). Here, $\tau_{r,XX}$ and $\tau_{A,XX}$ are, respectively, the radiative and the Auger lifetime of a biexciton (65). (C) Increasing splitting between the light and heavy hole states owing to biaxial strain leads to the reduction of the optical gain threshold, which facilitates the realization of cw lasing (69). (D) Continuously graded cQDs (cg-cQDs) exhibit strong suppression of Auger decay, which increases the biexciton emission efficiency and extends optical gain lifetimes. (E) A current-focusing LED architecture helps boost the current density to levels sufficient for achieving population inversion in a cQD active layer. (F) Light amplification by using cg-cQDs incorporated into a current-focusing LED (51).

the intragap transition involving the energy-accepting carrier (51). This enabled red-emitting LEDs with high droop-free EQEs up to $\sim 100,000$ cd m⁻² (Fig. 2G) (52). cQD surface modifications have been also pursued to facilitate balanced charge injection, enabling green-emitting LEDs with brightness $>400,000$ cd m⁻² (53). In addition to improving EQEs and brightness, good charge balance helps reduce heat generation by suppressing Auger decay, which is essential to maintaining high EQE stability and extending device longevity (54). Substan-

tial strides in cQD-LED performance have led to EQEs near the limit defined by the light extraction efficiency from a high-index semiconductor medium, exceeding 20% for red and green colors and 18% for blue (55–57).

The realization of efficient IR cQD LEDs—desired for technologies such as optical telecommunications, biological imaging, and chemical sensing—had previously been hindered by difficulty in obtaining simultaneously high-IR PLQY and highly efficient, balanced charge injection (58). The advent of cQD-in-perovskite

solids—cQDs embedded in a metal halide perovskite—provided an avenue to resolving these problems (59). These materials take advantage of ambipolar charge transport of perovskites and spectral tunability of the cQDs. The cQDs and the perovskite matrix form a defect-free epitaxial junction with a band alignment that can be tuned to facilitate carrier injection into the cQDs. This materials platform led to high-performance IR LEDs with good power conversion efficiencies (PCEs) and high brightness (60). The use of quantum-confined perovskite matrices, in which charges were injected as excitons, led to improved charge balance and helped further increase the EQE and the brightness (61). An alternative QD-in-matrix approach used inorganic bulk-heterojunction solids implemented by using percolated networks of PbS and ZnO nanocrystals to achieve a PCE of 9.3% (62).

QD lasers

Semiconductor lasers are sources of coherent light applied in numerous technologies, including optical communications, on-chip interconnects, digital projection systems, manufacturing, surgical instruments, metrology, and emerging quantum information technologies. Lasing requires population inversion in which the occupancy of a higher-energy state of the emitting transition exceeds that of a lower-energy state. For QDs with twofold-degenerate electron and hole band-edge states, the onset of population inversion and optical gain occurs when the average number of electron-hole pairs per-dot is one ($\langle N_{eh} \rangle = 1$) (63). This corresponds to the regime of optical transparency or optical-gain threshold when absorption and stimulated emission exactly compensate each other (Fig. 3A).

To enact optical gain, at least a fraction of the QDs in the sample must contain two or more excitons, implying that optical amplification in QD media relies on biexcitons and other higher-order multiexcitons. This greatly complicates the realization of lasing because of the extremely fast deactivation of optical gain through nonradiative Auger recombination (63, 64). Fast Auger decay represents an especially serious obstacle for realizing continuous-wave (cw) lasing. In particular, in the case of small-size standard (nonengineered) cQDs with <100 -ps Auger lifetimes, it leads to prohibitively high lasing thresholds of around 10^5 to 10^6 W cm⁻² (Fig. 3B) (65). As a result, most experimental demonstrations of cQD lasing used pulsed optical excitation (37).

The efforts to suppress Auger recombination explored “giant” CdSe/CdS cQDs with a thick shell to increase the spatial extent of electronic wave functions (66) and interfacial alloying to realize a “smooth” confinement potential (67, 68). These approaches enabled a considerable reduction of lasing thresholds in

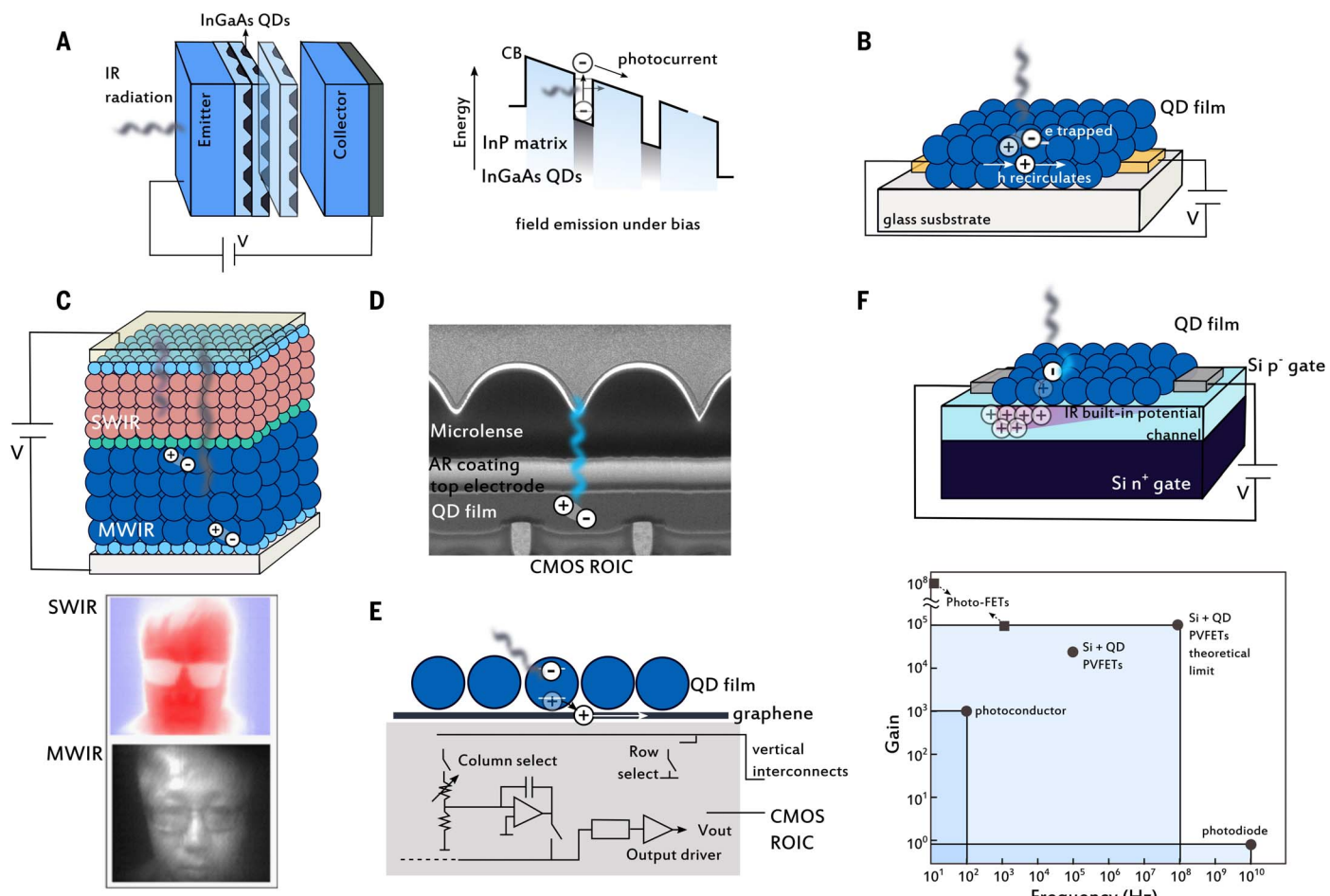


Fig. 4. QD materials for sensing. (A) Early QD photodetectors relied on field emission from III-V eQDs embedded into a wider-bandgap InP matrix where charge transport occurred. (B) The programmed surface modification and assembly of cQDs led to photoconductive cQD solids with high SWIR sensitivity (80). (C) Photodetection at the MWIR is challenging and typically achieved with HgTe cQDs. Shown here, a cQD back-to-back photodiode enables monolithic detection of SWIR and MWIR bands (85). (D) cQDs have been incorporated into Si-based

imaging technologies, enabling new sensing architectures such as top-surface photodetection: cQDs sensitize a Si CMOS readout-integrated-circuit (ROIC) (93). (E) The combination of cQDs with high-mobility materials such as graphene can provide large photoconductive gains. The integration of this sensing platform into CMOS has been recently reported (95). (F) cQDs have also been monolithically integrated with Si in a photovoltage transistor modulating charge transport in Si by use of an IR cQD-generated photovoltage (96).

the pulsed regime (65) and allowed for demonstrating cw lasing with pump powers of a few kilowatts per square centimeter (69). The latter study also took advantage of strong biaxial strain realized by means of epitaxial facet-selective growth of CdS on CdSe cores. This increased the energy splitting between valence-band states and helped impede thermal depopulation of the band-edge hole level involved in lasing (Fig. 3C).

The development of compositionally graded core-multishell cQDs have stimulated further advances in the lasing field (Fig. 3D) (37, 51). The electronic band alignment in these structures increases the spatial overlap between electron and hole wave functions and thus boosts the emission rate compared with quasi-type II CdSe/CdS systems. The radially graded composition also leads to strong suppression of Auger decay, which extends optical gain lifetimes. These properties have been exploited to

demonstrate electrically driven optical gain in “current-focusing” LEDs (Fig. 3, E and F) and to realize dual-function devices with an integrated optical cavity that operated as an optically pumped laser and a standard LED (70). These are major milestones on the path to electrically pumped cQD laser diodes.

Whereas cQD lasers are still at the stage of exploratory devices, lasers based on eQDs have already reached technological maturity (71). In particular, record-low thresholds (72) and high operating temperatures of up to 220°C (73) have been achieved by using III-V eQDs. eQD lasers have become a key component in silicon photonics, optical interconnects, telecommunication, and data centers (74).

QD materials for optical sensing and imaging

The wide spectral tunability of QD absorption, combined with good mobility of photogener-

ated charge carriers, make them competitive candidates for optical sensor applications for wavelengths beyond the Si bandgap. Early QD sensors relied on InGaAs eQDs grown on InP, in which photoexcited electrons were emitted into the InP transport matrix with the help of an electric field (Fig. 4A) (75). eQD IR detectors were then considered a compelling sensing platform of IR light (76), demonstrating low dark current and high sensitivity and speed (77, 78).

The high cost/performance tradeoff of existing IR sensors based on bulk narrow-gap semiconductors opened additional opportunities for cQDs, which have the benefit of readier integration with Si chips. Initial cQD IR sensors consisted of PbS cQDs embedded in a polymer matrix, in which a type II heterojunction provided selective charge circulation (79). Surface modification of cQDs enabled electrically coupled cQD solids with increased IR sensitivity

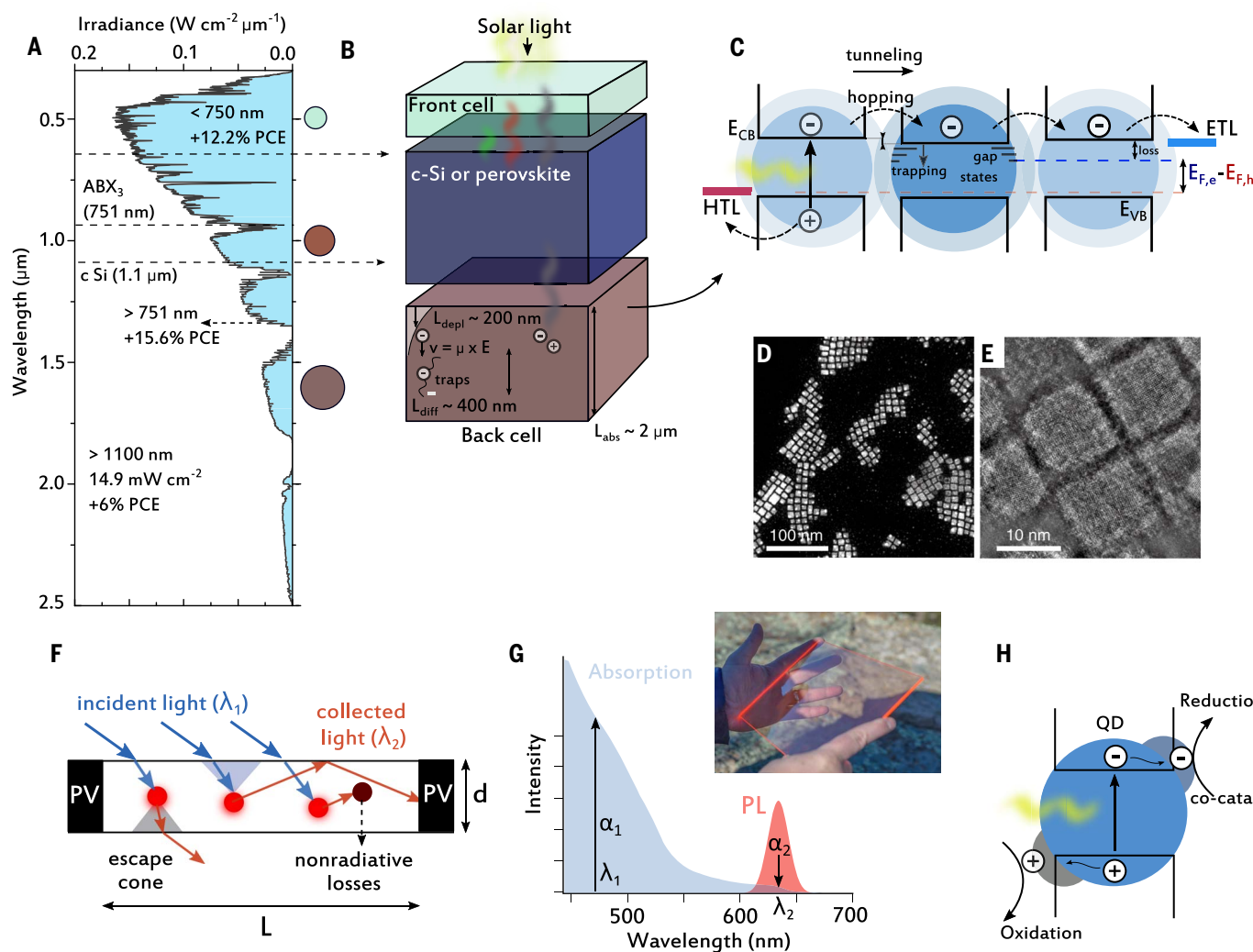


Fig. 5. QD semiconductors for solar energy harvesting. (A) Solar irradiance spectrum and cumulative power. (B) cQD absorption can be tuned across the entire solar spectrum, which is of interest for lightweight standalone solar cells or tandem cells to increase the net PCE of other technologies such as perovskites (additional +15.6% PCE) and cSi (+6% PCE). (C) Efficient photovoltaic operation in QD solids requires minimization of defects pinning quasi-Fermi level splitting and open-circuit voltage and sufficient QD coupling to facilitate charge transport to electron (ETL) and hole (HTL) transport electrodes. (D and E) Perovskite cQDs have emerged as a

strategy to achieve high-quality perovskite solids with stabilized composition and record PCE (113). (F) In an LSC, cQDs absorb incident sunlight and then reemit lower-energy photons that are captured by means of total internal reflection in an LSC slab and waveguided toward edge-mounted solar cells. (G) The LSC performance can be enhanced by increasing the LSC quality factor (Q_{LSC}), which is defined as the ratio of the absorption coefficients for incident (α_1) and reemitted (α_2) photons ($Q_{\text{LSC}} = \alpha_1 / \alpha_2$). [Inset courtesy of UbiQD.] (H) cQDs are candidates for photo- and electrocatalysts to store solar energy in the form of chemical bonds.

(Fig. 4B) (80). These devices exhibited high photoconductivity and specific detectivities (D^* ; noise-equivalent power normalized to measurement bandwidth and device area) comparable with those of III-V technologies. The high photoconductive gain—while one type of photocarrier is trapped, the other recirculates many times leading to gain—came with the downside of high dark currents and time response limited to approximately milliseconds.

Unlike photoconductors, photodiodes rely on the collection of minority carriers, opening the door to lower dark currents and faster time response. Advances in surface chemistry

enabled sensitive short-wavelength IR (SWIR) cQD-based photodiodes with 3-MHz 3-dB bandwidths but no gain (81).

Sensing of mid-IR wavelengths—of interest for spectroscopy, gas and health monitoring, aerospace, and thermal imaging—is more challenging. As the semiconductor bandgap decreases, it becomes closer to background radiation and transport energy barriers. This increases dark current and noise and makes charge collection by using conventional electronics more difficult. The materials choice for IR sensing is reduced to few candidates in the HgCdTe family, InSb, and III-V epitaxial

quantum-well structures exploiting intraband transitions that demand complex fabrication and low temperature for efficient operation. Compared with other technologies, such as bulk HgCdTe photodiodes or Schottky photo-emissive sensors, cQD-based IR sensors offer the prospect of lower dark currents, higher-temperature operation, and higher detectivity.

Improvements in colloidal synthesis of HgTe cQDs, doping, and surface engineering led to the demonstration of mid-IR sensors with room-temperature photoresponse beyond 5 μm (82–84). Multispectral IR detectors have been demonstrated by using two opposing

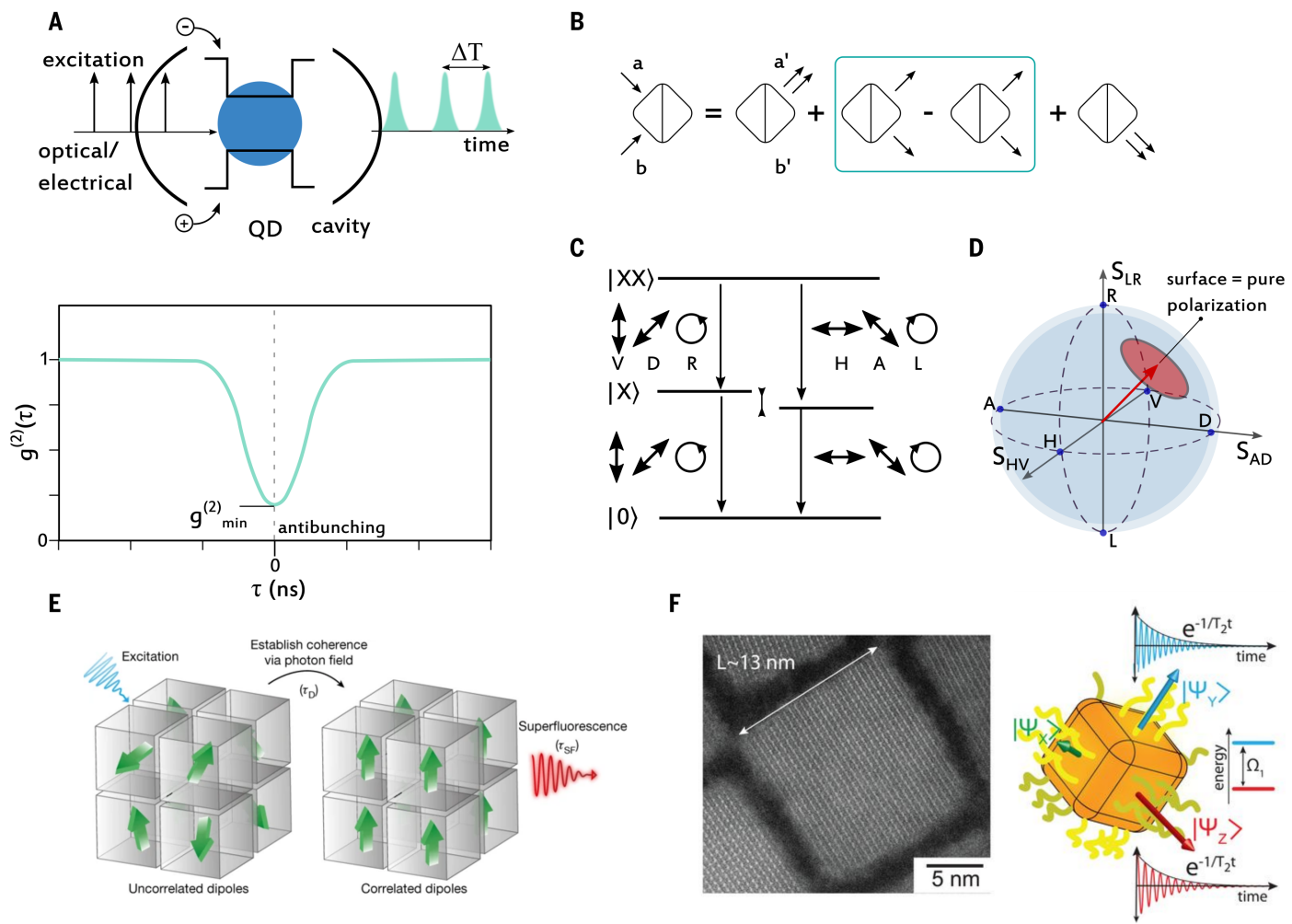


Fig. 6. QD materials for quantum light generation. (A) (Top) A single-photon source based on a QD coupled to a resonant cavity. (Bottom) The second-order intensity correlation function (g^2) exhibits an “antibunching dip” at time zero, a signature of high single-photon purity. (B) If two indistinguishable photons simultaneously reach a beam splitter, they leave it along the same optical path as a photon pair. This experiment is used to assess the degree of photon indistinguishability. (C) Generation

of polarization-entangled photon pairs through a “radiative cascade” produced by decay of a biexciton. (D) The degree of entanglement can be assessed with polarization tomography. Coherent interaction would lead to states on the surface of the Poincaré sphere. (E) Superfluorescence from colloidal CsPbX₃ ensembles (169). (F) Single-photon emission from CsPbX₃ QDs has been achieved with coherence times of tens of picoseconds (155).

Schottky junctions of cQDs with different bandgaps (Fig. 4C) (85). IR intraband photodetectors have also been demonstrated with doped cQDs (86–88) or mixtures of different cQDs (89).

Solution-processing of cQDs opened the door to their integration with incumbent visible sensor platforms such as Si complementary metal-oxide semiconductor (CMOS) readout electronics. In standard CMOS-based cameras, readout circuitry and photoactive elements coexist within the same layer, limiting the photodetection area (fill-factor) to ~30%. Top-surface integration of cQDs onto CMOS chips led to improved sensors with 100% fill-factor (Fig. 4D). The direct bandgap of cQDs also allowed for thinner photoactive films (~600 nm), reducing signal crossover from

adjacent pixels compared with silicon back-surface-illuminated sensors.

The integration of cQDs with materials that have high mobilities, such as metal halide perovskites, and 2D materials such as graphene and transition-metal chalcogenides enabled decoupling sensitization (light absorption) and charge transport (90). In QD-in-perovskite solids, it has been shown that one can combine the field emission of photoexcited charges from PbS cQDs into the perovskite matrix, along with ensuing charge transport within the higher-mobility perovskite matrix (91). cQDs and 2D materials have been incorporated in a phototransistor architecture (Fig. 4E). As photoexcited electron-hole pairs in the cQD layer split, one of the charges drifts into the 2D transport layer, where it recirculates multiple

times before recombination, leading to photoconductive gain (92). This mode of operation enables larger photoconductive gain than conventional cQD solids (because of faster charge recirculation) without compromising time response (93). However, it requires special integration with current CMOS technologies (94). CMOS sensor arrays modified to include graphene and PbS cQDs have achieved high on-chip detectivity from the visible to the IR (Fig. 4E) (95).

cQDs have also been integrated into Si transistors, modulating Si transport by means of a photovoltage effect (96). Light absorption within the PbS cQD layer leads to a modification of the depletion region in the Si layer, controlling transport in Si and extending its photoresponse up to 1500 nm. A comparison of performance

characteristics for different sensor architectures points to a favorable combination of gain and bandwidth in these devices (Fig. 4F).

The highly tunable emission of cQDs was exploited in alternative sensing schemes. Up-conversion devices transduce lower-energy photons (such as IR) into visible light, which is then directly imaged (97, 98); down-conversion devices convert high-energy radiation into lower-energy photons, which is of interest for detection of radiation such as x-rays. CsPbBr₃ perovskite cQDs have been used to realize inexpensive flexible scintillators with high performance (99). cQD tunability has also been exploited to realize fast spectrometers (100).

QD materials for solar energy harvesting

Solar energy harvesting is widely achieved by using photovoltaic Si modules, with impressive leveled costs below 2¢/kilowatt-hour (kWh) in well-isolated geographic regions, thus approaching grid parity. The high crystallinity of eQDs offers a path toward high-efficiency multijunction solar cells. cQDs can be deployed in single-junction lightweight solar cells or in tandem configurations to complement existing PV technologies (Fig. 5, A and B) and used as the photoactive material in LSCs and photocatalytic systems.

cQD solar cells

In cQD photovoltaic devices, the energy of photogenerated excitons is harvested in the form of electrons and holes, which are collected and used to generate an electric current. Early cQD solar cells relied on a dye-sensitized configuration as organic dye replacements. Electron-hole pairs were harvested by means of redox reactions and charge transport facilitated through TiO₂ and electrolyte. Initial solid-state cQD PV devices used PbS cQDs embedded in a conducting polymer to enable charge transport (101).

Improvements in charge transport in cQD solids opened the door to cQD active layers (Fig. 6C) (102). This was first implemented by using a Schottky junction configuration, in which the built-in field at the cQD-metal interface facilitated charge extraction. This was followed by other architectures such as the depleted heterojunction, which maximized field-assisted charge collection (103).

Higher-performance cQD solar cells would still require efficient charge extraction at near-flatband, maximum-power point conditions in which charge transport is diffusion-based rather than field-assisted. Because the diffusion length (L_{diff}) of minority carriers was shorter than the length required to maximize light absorption, this led to an absorption-extraction compromise. Extended L_{diff} required fewer defects in the cQD solid, to increase carrier lifetime and mobility, and avoidance of quasi-Fermi level and open-circuit voltage (V_{oc})

pinning—also curtailed by cQD polydispersity and disorder (104, 105).

Advances in cQD quality and PV PCE have been achieved through improvements in synthesis; ligand exchanges relying on small metal halides to improve cQD coupling, protect against oxidation, and reduce the density of defects (106); doping and surface dipole engineering (107); device architectures (103); and light management (108).

The implementation of cQD bulk heterojunction (BHJs)—percolating paths of cQDs forming a type II heterojunction (109)—offered a route to extend L_{diff} by separating electron and hole transport, reducing recombination. One challenge is the retention of the desired cQD configuration once the final solid is assembled. BHJs are also attractive to reduce V_{oc} deficit through DOS modification and remote passivation (62).

The introduction of single-step solution-phase ligand exchanges enabled to preserve cQD monodispersity in the final solid, leading to a more uniform energy landscape, reduced bandtail states, and improved charge transport, resulting in higher V_{oc} and PCE > 11% (110). Further improvements in cQD order and coupling achieved through perovskite bridging have been shown to boost PCE to >14% (111).

Advances in device architecture have led in parallel to similar PCEs. These exploited the combination of PbS cQDs with small-molecule organic semiconductor layers to complement cQD absorption and enhance charge extraction (112).

Rapid progress has been made in recent years using metal halide perovskite cQDs (Fig. 5, D and E). The use of presynthesized high-quality CsPbX₃ cQDs as the precursor to perovskite solids—as opposed to an on-substrate perovskite crystallization—has enabled control over perovskite phase stability. The lower density of electronic defects in perovskite cQD solids compared with PbS led to PCEs that reached 16.6% (113–115).

The tunable bandgap of cQDs can be exploited to augment the PCE of other PV architectures by harvesting IR light. This strategy can lead to up to +6 and +12% additional PCE points when combined with Si or perovskites, respectively (Fig. 5A). To date, PbS cQD:perovskite tandems have achieved a 24.7% PCE when combined in a four-terminal configuration (116).

Alternative strategies to improve PV performance include solar spectra reshaping, in which cQDs absorb and reemit light at a region of interest. CsPbX₃ cQDs doped with Yb³⁺ ions can efficiently absorb blue light and reemit in near-IR, with quantum efficiency approaching 200% (117).

Luminescent solar concentrators

LSCs are light-management devices envisioned as large-area sunlight collectors for building-

integrated solar cells (118). In LSCs, light is absorbed by fluorophores embedded in an optically transparent slab. Excited fluorophores reemit lower-energy photons, which are guided by means of total internal reflection to slab edges to be collected by PV modules (Fig. 5F). If the light-collecting area of the LSC is greater than the area of its edges, the output photon flux density (ϕ_{out}) can exceed the incident flux density (ϕ_{in}), concentrating light. In contrast to traditional lens- and mirror-based concentrators, LSCs can operate equally efficiently for direct and diffuse light, making them well suited as large-area sunlight collectors for building-integrated PVs installed as solar windows and solar sidings (119).

An important performance-limiting factor of LSCs is light reabsorption by the fluorophores themselves, which restrict the maximum device size. The interplay between sunlight-harvesting ability and losses due to reabsorption can be quantified by an LSC quality factor ($Q_{\text{LSC}} = \alpha_1/\alpha_2$), which is defined as the ratio of the absorption coefficients for the harvested (α_1) and the re-emitted (α_2) light (Fig. 5G). The maximum concentration factor ($C = \phi_{\text{out}}/\phi_{\text{in}}$) obtained in the large-area limit is approximately equal to Q_{LSC} , highlighting the importance of achieving $Q_{\text{LSC}} \gg 1$, which can be realized with engineered cQDs (120). An additional requirement is spectral matching between fluorophore's emission and PV absorption. In the case of Si PVs, this implies that for optimal LSC operation, cQDs should combine efficient NIR emission and a spectrally displaced NIR absorption onset.

Initial efforts to tackle reabsorption explored giant CdSe/CdS cQDs. A thick CdS shell served as a light-harvesting antenna that funneled photogenerated carriers into a small emitting CdSe core (121). Because the bandgap of the core is smaller than that of the shell, reemitted light is not attenuated by absorption arising from a large-volume shell. This approach enables Q_{LSC} of more than 100 and leads to high concentration factors exceeding ~60 (120, 122).

The amount of sunlight absorbed by giant CdSe/CdS cQDs is limited by the high bandgap of the shell. This problem has been addressed by using narrower-gap I-III-VI CuInSe_xS_{2-x} cQDs (123, 124). In addition to improved sunlight harvesting, these structures exhibit low reabsorption because of a peculiar light emission mechanism that involves an intragap hole-like state (125). Further improvements in the LSC efficiency have been obtained by exploiting spectral splitting in tandem devices implemented by using a combination of II-VI and I-III-VI cQDs (126).

Following principles exploited in LSCs, cQDs can be used for spectral reshaping of incident sunlight for applications in agriculture to match the absorption of photoactive molecules and thereby boosting crop growth. This approach

is presently being tested for greenhouse and indoor farming (127).

Photo- and electrocatalysis

Storage of renewable energy as chemical bonds—for example, transforming greenhouse gases or pollutants into fuels and chemical feedstock—is a path toward carbon-neutral energy systems (128). In this context, cQD materials might enable photon-to-chemical energy conversion across the solar spectrum, combining benefits of heterogeneous and homogeneous catalysis (129). cQDs can be used as standalone photocatalyst or as the sensitizing agent of metal catalytic sites.

In a photocatalytic system, excited electron-hole pairs in a semiconductor are directed from conduction and valence bands to catalytic sites to drive reduction and oxidation reactions, respectively (Fig. 5H). The cQD large surface-to-volume ratio offers a path to increased reaction rates. Strain and defect engineering was shown to increase cQD photocatalytic activity (130). Energy positioning is interesting to match the potentials of different reactions and control selectivity and to drive electrons and holes toward different reaction sites, minimizing product recombination. cQD surfaces can be manipulated to influence the interaction between solvents and adsorbates (131).

cQDs have been used in different photocatalytic systems, such as H₂/O₂ evolution (132) and CO₂ reduction (133), lignocellulose (134) and plastic (135) reforming, ammonia generation (136), and water purification (137). cQDs have also been implemented in hybrid strategies to sensitize living bio-organisms, enabling the production of CO₂-upgraded feedstock (138).

Carbon-based cQDs are an attractive route to realize metal-free photocatalysts. Their optical and electronic properties can be widely manipulated to control their size, shape, and doping (139). Their chemical inertness brings benefits in aqueous reactions at extreme pH conditions. Quantum-confined transition-metal dichalcogenides have also shown a path for water splitting and CO₂ reduction (140), among other reactions.

In water-supported reactions, single-junction photocatalytic systems must overcome the energy gap and overpotentials required to split water (>1.23 eV) and outcompete product recombination. This can be achieved through two-step excitation and Z-scheme energy transfer in cQD heterojunctions and using tandem photoelectrochemical (PEC) systems, in which redox reactions take place separately at the photocathode (anode). The design of photoelectrodes follows the same logic as that of photovoltaic systems but brings added challenges of cocatalyst integration and more demanding chemical stability. Further progress in PEC performance and system cost are still

required for this technology to have impact commercially (141).

Pure electrochemical systems have the advantage of separate optimization of PV and electrocatalyst modules. cQD heterostructures might enable a design platform to tailor the physical, chemical, and electronic properties of catalysts—which undergo extensive surface reconstruction through oxidation and reduction from their initial configuration as they are operated.

QD materials for quantum light generation

The development of QD technology for quantum computers and quantum communication is of growing interest. Quantum technologies are desirable for fast computation and secure communication (142). The artificial atom-like features of QDs triggered efforts to use them as quantum technology hardware, leveraging potential advantages such as ease of miniaturization, scalability, and integration.

Although the coherence properties of QD quantum bits are superior to higher-dimensional semiconductors (143–148), they so far have remained considerably behind those of atoms or other solid-state systems such as defect centers. For optically active excitons in self-assembled QDs, the coherence time can be as long as nanoseconds; for optically inactive excitons, it may reach microseconds, similar to spins.

QDs are attractive as quantum light sources, providing emission of single as well as entangled photons with high fidelity (149). Excellent performance parameters have been achieved, mostly by using eQD structures thus far. A key factor in that respect is the “silencing” of the quantum emitter environment—for example, by suppressing lattice vibrations and charge fluctuations. The first can be achieved with cryogenic cooling, whereas the second requires high material quality and separation from surfaces and surfactants located therein.

Single-photon sources

A QD in a high-quality optical resonator cavity is the basic unit of a single-photon source (Fig. 6A) (150). After tailored pulsed excitation, the QD will ideally emit one and only one photon, which is called antibunching. The quality of antibunching can be characterized by measuring the second-order correlation function $g^{(2)}(\tau = 0)$, which should reach zero in case of perfect operation because it gives the probability of detecting simultaneously two photons (Fig. 6A, bottom). Over the years, the continuous improvement of In(Ga)As/GaAs eQD materials (151, 152) has led to the suppression of $g^{(2)}(\tau = 0)$ to less than 10^{-4} (153). High-brightness In(Ga)As/InAs eQD single-photon sources have been accomplished by using optical (154, 155) or electrical (156) excitation with record-high operation frequencies of up to 1 GHz. Single-photon sources are usually

operated at cryogenic temperatures, but operation at room temperature or above is desired for practical quantum integrated circuit systems. On the basis of the large biexciton binding energy (>60 meV) realized in GaN eQDs embedded in a GaN/AlGaN nanowire, single-photon emission was achieved at 350 K (157).

In addition, photons emitted during a sequence of pulsed excitation should be indistinguishable (158), a requirement also for photon-based quantum simulators and computers that exploit Fock number states with a well-defined number of identical photons. Indistinguishability concerns their energy, polarization, and spatiotemporal mode structure and can be tested for two photons by means of a “which-path” experiment (Fig. 6B): When two indistinguishable photons simultaneously reach a 1:1 beam splitter, they leave this splitter only in pairs. This is due to destructive interference of the transition amplitudes for the two photons leaving the beam splitter through separate ports (159). Photon indistinguishability exceeding 98% has been achieved for eQD devices (160).

Sources of entangled photons

QDs can generate entangled photons (for example, by using their polarization degree of freedom through the biexciton cascade recombination) given a sufficiently small splitting of the polarized exciton states so that the photons cannot be distinguished through their energies (Fig. 6C) (161). The biexciton is a zero-angular-momentum eigenstate, so the polarizations of the two photons from the biexciton decay cancel. On the other hand, each photon can have either of the two possible complementary polarizations, leading to entanglement (Fig. 6D) (162–165). The fidelity of entanglement generation has already exceeded 98% (166). Efforts have been also made to generate cluster states with a photon number exceeding two (167).

Remaining goals include further enhancement of photon source and detector performance parameters and integration into nanophotonic circuits. Currently, operation has been limited to cryogenic temperatures. Another priority to achieve greater impact is the demonstration of similarly high-fidelity performance in the fiber-based telecommunication wavelength range, which is around 1.5 μm.

Colloidal QDs for quantum light generation

QD quantum light sources have largely relied on eQDs, even though one of the very first demonstrations of antibunching involving QDs used colloidal nanocrystals (168). Ordered superlattices of CsPbX₃ perovskite nanocrystals have been shown to achieve superfluorescence light generation (169), potentially opening the door to the implementation of multiphoton entangled quantum light sources (Fig. 6E).

Individual CsPbX_3 QDs have been used to demonstrate highly tunable single-photon sources (155) that, combined with their solution processability, results in a compelling material platform to serve as the building blocks of next-generation quantum light sources (Fig. 6F).

Challenges and outlook

Furthering technological impact of QDs will require continued advances on multiple fronts, including QD synthesis and assembly, integration with existing technological platforms, and the development of effective QD-specific device designs.

From a synthetic perspective, the realization of high-quality cQD materials based on solution-chemistry syntheses that transition toward widely available, inexpensive precursors and solvents is of increasing importance (170, 171). Scaling up synthesis processes is required to meet the large-volume material demands of markets in consumer electronics, wearable devices, displays, and energy generation and storage. Broad adoption of cQD devices will put additional pressure on reducing the manufacturing costs of highly monodisperse cQDs.

The cost to volume and availability of precursors have a strong impact on the final cost as production scales up. The available body of knowledge on cQD synthesis suggests that it should be possible to switch from currently used costly trimethylsilyl-based chalcogenide and pnictide precursors with poor atom economy (172) to simpler species, such as H_2S and PH_3 . Other approaches, such as the use of amine complexes or thiourea, offer promising cQD quality and a path for greener synthesis with lower projected costs (170). Sustainable large-scale synthesis should consider recycling the large volume of organic solvents used during synthesis and cQD assembly to decrease their cost and associated carbon footprint (171). The implementation of continuous-flow automated syntheses is expected to bring down production costs substantially. Generally, cQD synthesis will benefit from the development of quantitative kinetic models based on the mechanistic understanding of each reaction step. Recent developments in machine learning and artificial intelligence can be implemented to increase the predictive power of these models (173).

The regulation of heavy metals such as Pb, Cd, and Hg, among others, requires advancing the synthesis, processes, and performance of more widely accepted cQD materials. Widespread technological adoption brings additional constraints and challenges. Many groundbreaking fundamental studies have used CdSe cQDs and Cd-based core shell structures. In terms of color purity and other performance metrics, CdSe cQDs are superior to cQDs of InP , $\text{CuInSe}_{2-x}\text{S}_x$, and other less toxic semi-

conductors. However, legislative regulations, additional manufacturing and transportation costs, and environmental concerns have required displays to switch to InP cQDs. One can anticipate a similar trend with other emerging cQD technologies. Substantial progress has been achieved by using Cu-, Bi-, Sn-, Sb-, and In-based cQDs in display and energy-harvesting applications (174–176). Accelerated materials discovery is also expected to play an increasing role in these areas (177). Another important direction for cQD synthesis will be the development of new routes toward III-V cQDs beyond currently available InP, InAs, and InSb. The record-performing eQD devices all used Ga-based materials such as GaAs and GaN, which are very difficult to synthesize with current solution methods.

Long-term material stability is an additional metric that needs careful study when proof-of-concept demonstrations are successful. In general, nanomaterials are metastable with respect to bulk crystals. This raises an important problem of their morphological and chemical stability during operation—often at elevated temperatures. An increased understanding of sintering and grain growth in materials composed of <10 -nm semiconductor grains is needed (178). Generally, covalent semiconductors show fewer tendencies to electromigration, ion diffusion, and sintering compared with those of ionic compounds. Lattice-matched cQD-in-perovskite systems have been shown to extend the lifetime of the cQDs and perovskite matrix and enhance their properties (179), representing a promising path forward.

From a manufacturing perspective, more efforts are needed to demonstrate reproducible cQD devices with high performance by using techniques such as roll-to-roll and spray casting. Patterning of cQD layers is an important step for manufacturing almost any electronic or optoelectronic device containing cQDs. The development of material- and process-tailored patterning methods will be critical for cQD technologies (180). Inkjet printing colloidal solutions offers exciting opportunities for device manufacturing, but patterns with $<10\text{-}\mu\text{m}$ features will require different, typically lithographic methods, such as direct optical lithography of functional nanomaterials (181). The translation of existing cQD surface chemistries—mostly developed at smaller scales or optimized for other deposition processes—to these manufacturing conditions is not trivial (103). The integration of cQD technologies in manufacturing processes of products with increasing complexity may bring additional challenges regarding cQD stability.

At the device level, the evaluation of performance metrics at conditions relevant to the final application and standardized stress tests combined with material degradation

studies are needed to advance in the reliability of cQD devices.

Challenges remain on the path to commercialization of cQD LEDs. So far, the best-performing devices still rely on Cd or Pb, which are highly toxic heavy metals. Another challenge is the need for pixelation of cQDs toward high-resolution, multicolor-LED-based displays. Different variations of photolithographic and printing techniques have been explored for this purpose but have yet to fully meet resolution, fidelity, and throughput requirements (182). LEDs based on cQDs must target further increases in power efficiency and stability at relevant operating currents and brightness. This is especially the case for UV, blue, and infrared LEDs, whose performance is lower than that for green and red colors.

The demonstration of electrically driven cQD laser diodes is an important present objective. Further advances in the design and implementation of complex cQD heterostructures are expected to help accomplish this goal. Interesting opportunities are associated with cQD-specific recent lasing concepts that do not require biexcitons to achieve optical gain. These include single-exciton gain (183) and charged-exciton gain (184–186). Promising results have been also obtained with emerging nanocrystalline materials such as CsPbX_3 perovskite cQDs (187) and quasi-2D nanoplatelets (188, 189). Recently, cQD optical gain and amplified spontaneous emission were realized within the IR telecom window by using PbS cQDs (190).

Challenges also remain in the area of eQD lasers. Improvements in eQD fabrication (S-K growth) are needed to increase the in-plane density of QDs and number of layers in the stack without compromising materials quality and QD uniformity. These are expected to provide with extended high-temperature stability of the threshold current, increased modulation bandwidth, and reduced noise features that are important for quantum light applications. Lasers that use droplet eQDs have yet to be demonstrated.

In addition, it is interesting to develop eQD lasers that are based on other materials. In particular, the realization of efficient ultraviolet GaN eQD lasers would open the door to manufacturing and lithography applications. The fabrication of eQD lasers on CMOS-compatible silicon-on-insulator substrates is also an important unresolved challenge.

In photodetection, deepened understanding of cQD assembly, charge transport, intragap states, and interfaces are needed to improve the sensitivity of sensors operating at the SWIR and beyond (191). Mobilities beyond $10\text{ cm}^2\text{ V}^{-1}\text{ s}^{-1}$ and low dielectric constants are desired to meet the demands of fast sensing ($<1\text{ ns}$) for time-of-flight 3D imaging and light detection and ranging (LIDAR)—which is of

interest to the expanding autonomous driving industry (93), machine vision, and augmented reality for consumer electronics. Efforts to improve device architecture (92), charge mobility, and trap density in cQD films are necessary to improve D^* and response time (192).

Attention is still needed to increase the PCE and stability of cQD solar cells. Improvements in diffusion length need to be pursued together with strategies to ensure long-term chemical and mechanical compatibility with other elements in tandem devices. Because IR harvesting requires larger-diameter cQDs that have a different facet distribution, different surface chemistry strategies are needed relative to those used for smaller cQDs (193). Multiple exciton generation or carrier multiplication, in which one high-energy photon ($E > 2E_g$) generates multiple electron-hole pairs (194), remains a path to be fulfilled for achieving PCEs that exceed a traditional Shockley-Queisser limit. Long-term stability at maximum power point and under temperature and humidity, which is now standard in perovskite PV reports (195), needs to be consistently reported to evaluate the impact of this technology and guide its further development.

In the context of eQDs, the realization of devices that achieve high uniformity, high density, and multiple layers has the prospect to enable ultrahigh-efficiency solar cells with near 80% PCE by using multiple intermediate levels (196).

The largest cQD-based LSCs are yet within a few tens of square centimeters (197). An important challenge is the scale-up of these proof-of-principle structures to meter-sized devices that would be of relevance for building-integrated sunlight collectors. This will require further CQD developments to improve the LSC-relevant parameters (such as PLQY and Q_{LSC}), especially in the case of NIR emitters. Other challenges include the elimination of propagation losses in the LSC waveguide and the enhancement of device stability under outdoor conditions.

The use of cQDs in photo- and electrochemistry is still in its early stages. It is still to be seen which cQD properties can be exploited in practical systems, demanding long-term stability at harsh electrochemical conditions.

In the application of QDs to nonclassical quantum light sources such as single-photon and entangled-photon sources, high-precision position and wavelength control and integration to a quantum circuit are important issues. Nonclassical quantum light sources are positioned as indispensable devices for quantum key distribution and quantum repeater systems for quantum communication. Emerging distributed quantum computer systems (edge quantum computing systems) will be mutually connected by quantum networks. In that case, quantum communication based on on-demand

and highly efficient nonclassical quantum light sources will play large roles.

In addition, quantum bits (qubits) based on semiconductor QDs are one of key candidates for realizing quantum computer systems. Up to now, these have been realized by using QDs under depletion effect induced by electric fields. eQDs relying on group IV such as silicon or germanium are emerging as next-generation qubits. The application of QDs for quantum sensing and metrology could also enable QDs to replace diamond nitrogen-vacancy centers and carbon nanotubes.

REFERENCES AND NOTES

1. A. Y. Cho, J. R. Arthur, Molecular beam epitaxy. *Prog. Solid State Chem.* **10**, 157–191 (1975). doi: [10.1016/0079-6786\(75\)90005-9](https://doi.org/10.1016/0079-6786(75)90005-9)
2. A. P. Alivisatos, A. L. Harris, N. J. Levinos, M. L. Steigerwald, L. E. Brus, Electronic states of semiconductor clusters: Homogeneous and inhomogeneous broadening of the optical spectrum. *J. Chem. Phys.* **89**, 4001–4011 (1988). doi: [10.1063/1.454833](https://doi.org/10.1063/1.454833)
3. V. I. Klimov, Multicarrier interactions in semiconductor nanocrystals in relation to the phenomena of Auger recombination and carrier multiplication. *Annu. Rev. Condens. Matter Phys.* **5**, 285–316 (2014). doi: [10.1146/annurev-conmatphys-031113-133900](https://doi.org/10.1146/annurev-conmatphys-031113-133900)
4. A. I. Ekimov, A. A. Onushchenko, Quantum size effect in three-dimensional microscopic semiconductor crystals. *JETP Lett.* **34**, 345 (1981).
5. R. Rossetti, S. Nakahara, L. E. Brus, Quantum size effects in the redox potentials, resonance Raman spectra, and electronic spectra of CdS crystallites in aqueous solution. *J. Chem. Phys.* **79**, 1086–1088 (1983). doi: [10.1063/1.445834](https://doi.org/10.1063/1.445834)
6. L. Brus, Electronic wave functions in semiconductor clusters: Experiment and theory. *J. Phys. Chem.* **90**, 2555–2560 (1986). doi: [10.1021/100403a003](https://doi.org/10.1021/100403a003)
7. Y. Arakawa, H. Sakaki, Multidimensional quantum well laser and temperature dependence of its threshold current. *Appl. Phys. Lett.* **40**, 939–941 (1982). doi: [10.1063/1.92959](https://doi.org/10.1063/1.92959)
8. Y. Arakawa, H. Sakaki, M. Nishioka, H. Okamoto, N. Miura, Spontaneous emission characteristics of quantum well lasers in strong magnetic fields—An approach to quantum-well-box light source. *Jpn. J. Appl. Phys.* **22**, L804–L806 (1983). doi: [10.1143/JJAP.22.L804](https://doi.org/10.1143/JJAP.22.L804)
9. L. Goldstein, F. Glas, J. Y. Marzin, M. N. Charasse, G. Le Roux, Growth by molecular beam epitaxy and characterization of InAs/GaAs strained-layer superlattices. *Appl. Phys. Lett.* **47**, 1099–1101 (1985). doi: [10.1063/1.96342](https://doi.org/10.1063/1.96342)
10. D. Leonard, M. Krishnamurthy, C. M. Reaves, S. P. Denbaars, P. M. Petroff, Direct formation of quantum-sized dots from uniform coherent islands of InGaAs on GaAs surfaces. *Appl. Phys. Lett.* **63**, 3203–3205 (1993). doi: [10.1063/1.110199](https://doi.org/10.1063/1.110199)
11. J. Oshinowo, M. Nishioka, S. Ishida, Y. Arakawa, Highly uniform InGaAs/GaAs quantum dots (~15 nm) by metalorganic chemical vapor deposition. *Appl. Phys. Lett.* **65**, 1421–1423 (1994). doi: [10.1063/1.112070](https://doi.org/10.1063/1.112070)
12. M. Gurioli, Z. Wang, A. Rastelli, T. Kuroda, S. Sanguineti, Droplet epitaxy of semiconductor nanostructures for quantum photonic devices. *Nat. Mater.* **18**, 799–810 (2019). doi: [10.1038/s41563-019-0355-y](https://doi.org/10.1038/s41563-019-0355-y); pmid: [31086322](https://pubmed.ncbi.nlm.nih.gov/31086322/)
13. M. Bayer, Bridging two worlds: Colloidal versus epitaxial quantum dots. *Ann. Phys.* **531**, 1900039 (2019). doi: [10.1002/andp.201900039](https://doi.org/10.1002/andp.201900039)
14. C. B. Murray, D. J. Norris, M. G. Bawendi, Synthesis and characterization of nearly monodisperse CdE (E = sulfur, selenium, tellurium) semiconductor nanocrystallites. *J. Am. Chem. Soc.* **115**, 8706–8715 (1993). doi: [10.1021/ja0002025](https://doi.org/10.1021/ja0002025)
15. M. L. Steigerwald, L. E. Brus, Semiconductor crystallites: A class of large molecules. *Acc. Chem. Res.* **23**, 183–188 (1990). doi: [10.1021/ar0174a003](https://doi.org/10.1021/ar0174a003)
16. O. I. Micic, C. J. Curtis, K. M. Jones, J. R. Sprague, A. J. Nozik, Synthesis and characterization of InP quantum dots. *J. Phys. Chem.* **98**, 4966–4969 (1994). doi: [10.1021/j100070a004](https://doi.org/10.1021/j100070a004)
17. F. W. Wise, Lead salt quantum dots: The limit of strong quantum confinement. *Acc. Chem. Res.* **33**, 773–780 (2000). doi: [10.1021/ar970220q](https://doi.org/10.1021/ar970220q); pmid: [11087314](https://pubmed.ncbi.nlm.nih.gov/11087314/)
18. R. A. Bley, S. M. Kauzlarich, A low-temperature solution phase route for the synthesis of silicon nanoclusters. *J. Am. Chem. Soc.* **118**, 12461–12462 (1996). doi: [10.1021/ja962787s](https://doi.org/10.1021/ja962787s)
19. D. D. Vaughn 2nd, R. E. Schaak, Synthesis, properties and applications of colloidal germanium and germanium-based nanomaterials. *Chem. Soc. Rev.* **42**, 2861–2879 (2013). doi: [10.1039/C2CS35364D](https://doi.org/10.1039/C2CS35364D); pmid: [23128962](https://pubmed.ncbi.nlm.nih.gov/23128962/)
20. F. Wang et al., One-step synthesis of highly luminescent carbon dots in noncoordinating solvents. *Chem. Mater.* **22**, 4528–4530 (2010). doi: [10.1021/cm101350u](https://doi.org/10.1021/cm101350u)
21. L. Protesescu et al., Nanocrystals of cesium lead halide perovskites (CsPbX₃, X = Cl, Br, and I): Novel optoelectronic materials showing bright emission with wide color gamut. *Nano Lett.* **15**, 3692–3696 (2015). doi: [10.1021/nl5048779](https://doi.org/10.1021/nl5048779); pmid: [26533588](https://pubmed.ncbi.nlm.nih.gov/26533588/)
22. C. B. Murray, C. R. Kagan, M. G. Bawendi, Synthesis and characterization of monodisperse nanocrystals and close-packed nanocrystal assemblies. *Annu. Rev. Mater. Sci.* **30**, 545–610 (2000). doi: [10.1146/annurev.matsci.30.1545](https://doi.org/10.1146/annurev.matsci.30.1545)
23. M. C. Weidman, M. E. Beck, R. S. Hoffman, F. Prins, W. A. Tisdale, Monodisperse, air-stable PbS nanocrystals via precursor stoichiometry control. *ACS Nano* **8**, 6363–6371 (2014). doi: [10.1021/nm018654](https://doi.org/10.1021/nm018654); pmid: [24840645](https://pubmed.ncbi.nlm.nih.gov/24840645/)
24. D. J. Norris, A. L. Efros, S. C. Erwin, Doped nanocrystals. *Science* **319**, 1776–1779 (2008). doi: [10.1126/science.1143802](https://doi.org/10.1126/science.1143802); pmid: [18369131](https://pubmed.ncbi.nlm.nih.gov/18369131/)
25. D. Mocatta et al., Heavily doped semiconductor nanocrystal quantum dots. *Science* **332**, 77–81 (2011). doi: [10.1126/science.1196321](https://doi.org/10.1126/science.1196321); pmid: [21454783](https://pubmed.ncbi.nlm.nih.gov/21454783/)
26. D. Yu, C. Wang, P. Guyot-Sionnest, n-Type conducting CdSe nanocrystal solids. *Science* **300**, 1277–1280 (2003). doi: [10.1126/science.1084424](https://doi.org/10.1126/science.1084424); pmid: [12764194](https://pubmed.ncbi.nlm.nih.gov/12764194/)
27. M. A. Boles, D. Ling, T. Hyeon, D. V. Talapin, The surface science of nanocrystals. *Nat. Mater.* **15**, 141–153 (2016). doi: [10.1038/nmat4526](https://doi.org/10.1038/nmat4526); pmid: [26796733](https://pubmed.ncbi.nlm.nih.gov/26796733/)
28. M. C. Weidman, D.-M. Smilgies, W. A. Tisdale, Kinetics of the self-assembly of nanocrystal superlattices measured by real-time in situ x-ray scattering. *Nat. Mater.* **15**, 775–781 (2016). doi: [10.1038/nmat4600](https://doi.org/10.1038/nmat4600); pmid: [26998914](https://pubmed.ncbi.nlm.nih.gov/26998914/)
29. E. V. Shevchenko, D. V. Talapin, N. A. Kotov, S. O'Brien, C. B. Murray, Structural diversity in binary nanoparticle superlattices. *Nature* **439**, 55–59 (2006). doi: [10.1038/nature04414](https://doi.org/10.1038/nature04414); pmid: [16397494](https://pubmed.ncbi.nlm.nih.gov/16397494/)
30. C. B. Murray, C. R. Kagan, M. G. Bawendi, Self-organization of CdSe nanocrystallites into three-dimensional quantum dot superlattices. *Science* **270**, 1335–1338 (1995). doi: [10.1126/science.270.5240.1335](https://doi.org/10.1126/science.270.5240.1335)
31. M. P. Boneschanscher et al., Long-range orientation and atomic attachment of nanocrystals in 2D honeycomb superlattices. *Science* **344**, 1377–1380 (2014). doi: [10.1126/science.1252642](https://doi.org/10.1126/science.1252642); pmid: [24948734](https://pubmed.ncbi.nlm.nih.gov/24948734/)
32. Y. Nagaoka et al., Superstructures generated from truncated tetrahedral quantum dots. *Nature* **561**, 378–382 (2018). doi: [10.1038/s41586-018-0512-5](https://doi.org/10.1038/s41586-018-0512-5); pmid: [30232427](https://pubmed.ncbi.nlm.nih.gov/30232427/)
33. X. Jin et al., Cation exchange assisted synthesis of ZnCdSe/ZnSe quantum dots with narrow emission line widths and near-unity photoluminescence quantum yields. *Chem. Commun.* **56**, 6130–6133 (2020). doi: [10.1039/D0CC01302A](https://doi.org/10.1039/D0CC01302A); pmid: [32364191](https://pubmed.ncbi.nlm.nih.gov/32364191/)
34. BT Series, 2100: Image parameter values for high dynamic range television for use in production and international programme exchange; www.itu.int/rec/R-REC-BT.2100-2-201807-1/en.
35. D. A. Hanifi et al., Redefining near-unity luminescence in quantum dots with photothermal threshold quantum yield. *Science* **363**, 1199–1202 (2019). doi: [10.1126/science.aat3803](https://doi.org/10.1126/science.aat3803); pmid: [3087250](https://pubmed.ncbi.nlm.nih.gov/3087250/)
36. F. Meinardi, F. Bruni, S. Brovelli, Luminescent solar concentrators for building-integrated photovoltaics. *Nat. Rev. Mater.* **2**, 17072 (2017). doi: [10.1038/natrevmats.2017.72](https://doi.org/10.1038/natrevmats.2017.72)
37. Y.-S. Park, J. Roh, B. T. Diroll, R. D. Schaller, V. I. Klimov, Colloidal quantum dot lasers. *Nat. Rev. Mater.* **6**, 382–401 (2021). doi: [10.1038/s41578-020-00274-9](https://doi.org/10.1038/s41578-020-00274-9)
38. J. Owen, The coordination chemistry of nanocrystal surfaces. *Science* **347**, 615–616 (2015). doi: [10.1126/science.1259924](https://doi.org/10.1126/science.1259924); pmid: [25657234](https://pubmed.ncbi.nlm.nih.gov/25657234/)
39. I. L. Medintz, H. T. Uyeda, E. R. Goldman, H. Mattoussi, Quantum dot bioconjugates for imaging, labelling and sensing. *Nat. Mater.* **4**, 435–446 (2005). doi: [10.1038/nmat1390](https://doi.org/10.1038/nmat1390); pmid: [15928695](https://pubmed.ncbi.nlm.nih.gov/15928695/)
40. N. Yazdani et al., Charge transport in semiconductors assembled from nanocrystal quantum dots. *Nat. Commun.* **11**, 2852 (2020). doi: [10.1038/s41467-020-16560-7](https://doi.org/10.1038/s41467-020-16560-7); pmid: [32503965](https://pubmed.ncbi.nlm.nih.gov/32503965/)

41. C. Giansante, I. Infante, Surface traps in colloidal quantum dots: A combined experimental and theoretical perspective. *J. Phys. Chem. Lett.* **8**, 5209–5215 (2017). doi: [10.1021/acs.jpclett.7b02193](https://doi.org/10.1021/acs.jpclett.7b02193); pmid: [28972763](https://pubmed.ncbi.nlm.nih.gov/28972763/)
42. N. Yazdani *et al.*, Charge transport in semiconductors assembled from nanocrystals. *Nat. Commun.* **10**, 1038/s41467-020-16560-7 (2019).
43. D. V. Talapin, C. B. Murray, PbSe nanocrystal solids for n- and p-channel thin film field-effect transistors. *Science* **310**, 86–89 (2005). doi: [10.1126/science.1116703](https://doi.org/10.1126/science.1116703); pmid: [16210533](https://pubmed.ncbi.nlm.nih.gov/16210533/)
44. J.-S. Lee, M. V. Kovalenko, J. Huang, D. S. Chung, D. V. Talapin, Band-like transport, high electron mobility and high photoconductivity in all-inorganic nanocrystal arrays. *Nat. Nanotechnol.* **6**, 348–352 (2011). doi: [10.1038/nano.2011.46](https://doi.org/10.1038/nano.2011.46); pmid: [21516091](https://pubmed.ncbi.nlm.nih.gov/21516091/)
45. X. Lan *et al.*, Quantum dot solids showing state-resolved band-like transport. *Nat. Mater.* **19**, 323–329 (2020). doi: [10.1038/s41563-019-0582-2](https://doi.org/10.1038/s41563-019-0582-2); pmid: [31988516](https://pubmed.ncbi.nlm.nih.gov/31988516/)
46. H. Chen, J. He, S.-T. Wu, Recent advances on quantum-dot-enhanced liquid-crystal displays. *IEEE J. Sel. Top. Quantum Electron.* **23**, 1–11 (2017).
47. B.-L. Huang *et al.*, Color converting film with quantum-dots for the liquid crystal displays based on inkjet printing. *IEEE Photonics J.* **11**, 1–9 (2019). doi: [10.1109/JPHOT.2019.2911308](https://doi.org/10.1109/JPHOT.2019.2911308)
48. W. K. Bae, S. Brovelli, V. I. Klimov, Spectroscopic insights into the performance of quantum dot light-emitting diodes. *MRS Bull.* **38**, 721–730 (2013). doi: [10.1557/mrs.2013.182](https://doi.org/10.1557/mrs.2013.182)
49. J. M. Caruge, J. E. Halpert, V. Wood, V. Bulović, M. G. Bawendi, Colloidal quantum-dot light-emitting diodes with metal-oxide charge transport layers. *Nat. Photonics* **2**, 247–250 (2008). doi: [10.1038/nphoton.2008.34](https://doi.org/10.1038/nphoton.2008.34)
50. B. S. Mashford *et al.*, High-efficiency quantum-dot light-emitting devices with enhanced charge injection. *Nat. Photonics* **7**, 407–412 (2013). doi: [10.1038/nphoton.2013.70](https://doi.org/10.1038/nphoton.2013.70)
51. J. Lim, Y.-S. Park, V. I. Klimov, Optical gain in colloidal quantum dots achieved with direct-current electrical pumping. *Nat. Mater.* **17**, 42–49 (2018). doi: [10.1038/nmat5011](https://doi.org/10.1038/nmat5011); pmid: [29180770](https://pubmed.ncbi.nlm.nih.gov/29180770/)
52. J. Lim, Y.-S. Park, K. Wu, H. J. Yun, V. I. Klimov, Droop-free colloidal quantum dot light-emitting diodes. *Nano Lett.* **18**, 6645–6653 (2018). doi: [10.1021/acs.nanolett.8b03457](https://doi.org/10.1021/acs.nanolett.8b03457); pmid: [30198267](https://pubmed.ncbi.nlm.nih.gov/30198267/)
53. X. Li *et al.*, Bright colloidal quantum dot light-emitting diodes enabled by efficient chlorination. *Nat. Photonics* **12**, 159–164 (2018). doi: [10.1038/s41566-018-0105-8](https://doi.org/10.1038/s41566-018-0105-8)
54. X. Dai, Y. Deng, X. Peng, Y. Jin, Quantum-Dot Light-Emitting Diodes for large-area displays: Towards the dawn of commercialization. *Adv. Mater.* **29**, 1607022 (2017). doi: [10.1002/adma.201607022](https://doi.org/10.1002/adma.201607022); pmid: [28256780](https://pubmed.ncbi.nlm.nih.gov/28256780/)
55. X. Dai *et al.*, Solution-processed, high-performance light-emitting diodes based on quantum dots. *Nature* **515**, 96–99 (2014). doi: [10.1038/nature13829](https://doi.org/10.1038/nature13829); pmid: [25363773](https://pubmed.ncbi.nlm.nih.gov/25363773/)
56. H. Shen *et al.*, Visible quantum dot light-emitting diodes with simultaneous high brightness and efficiency. *Nat. Photonics* **13**, 192–197 (2019). doi: [10.1038/s41566-019-0364-z](https://doi.org/10.1038/s41566-019-0364-z)
57. O. Wang *et al.*, High-efficiency, deep blue ZnCdS/Cd_{1-x}S/ZnS quantum-dot-light-emitting devices with an EQE exceeding 18%. *Nanoscale* **10**, 5650–5657 (2018). doi: [10.1039/C7NR09175C](https://doi.org/10.1039/C7NR09175C); pmid: [29528343](https://pubmed.ncbi.nlm.nih.gov/29528343/)
58. D. Bozyigit, O. Yarema, V. Wood, Origins of low quantum efficiencies in quantum dot LEDs. *Adv. Funct. Mater.* **23**, 3024–3029 (2013). doi: [10.1002/adfm.201203191](https://doi.org/10.1002/adfm.201203191)
59. Z. Ning *et al.*, Quantum-dot-in-perovskite solids. *Nature* **523**, 324–328 (2015). doi: [10.1038/nature14563](https://doi.org/10.1038/nature14563); pmid: [26178963](https://pubmed.ncbi.nlm.nih.gov/26178963/)
60. X. Gong *et al.*, Highly efficient quantum dot near-infrared light-emitting diodes. *Nat. Photonics* **10**, 253–257 (2016). doi: [10.1038/nphoton.2016.11](https://doi.org/10.1038/nphoton.2016.11)
61. L. Gao *et al.*, Efficient near-infrared light-emitting diodes based on quantum dots in layered perovskite. *Nat. Photonics* **14**, 227–233 (2020). doi: [10.1038/s41566-019-0577-1](https://doi.org/10.1038/s41566-019-0577-1)
62. S. Pradhan *et al.*, High-efficiency colloidal quantum dot infrared light-emitting diodes via engineering at the supra-nanocrystalline level. *Nat. Nanotechnol.* **14**, 72–79 (2019). doi: [10.1038/s41565-018-0312-y](https://doi.org/10.1038/s41565-018-0312-y); pmid: [30510279](https://pubmed.ncbi.nlm.nih.gov/30510279/)
63. V. I. Klimov *et al.*, Optical gain and stimulated emission in nanocrystal quantum dots. *Science* **290**, 314–317 (2000). doi: [10.1126/science.290.5490.314](https://doi.org/10.1126/science.290.5490.314); pmid: [1030645](https://pubmed.ncbi.nlm.nih.gov/1030645/)
64. V. I. Klimov, A. A. Mikhailovsky, D. W. McBranch, C. A. Leatherdale, M. G. Bawendi, Quantization of multiparticle Auger rates in semiconductor quantum dots. *Science* **287**, 1011–1013 (2000). doi: [10.1126/science.287.5455.1011](https://doi.org/10.1126/science.287.5455.1011); pmid: [10669406](https://pubmed.ncbi.nlm.nih.gov/10669406/)
65. Y.-S. Park, W. K. Bae, T. Baker, J. Lim, V. I. Klimov, Effect of auger recombination on lasing in heterostructured quantum dots with engineered core/shell interfaces. *Nano Lett.* **15**, 7319–7328 (2015). doi: [10.1021/acs.nanolett.5b02595](https://doi.org/10.1021/acs.nanolett.5b02595); pmid: [26397312](https://pubmed.ncbi.nlm.nih.gov/26397312/)
66. F. García-Santamaría *et al.*, Suppressed auger recombination in “giant” nanocrystals boosts optical gain performance. *Nano Lett.* **9**, 3482–3488 (2009). doi: [10.1021/nl901681d](https://doi.org/10.1021/nl901681d); pmid: [19505082](https://pubmed.ncbi.nlm.nih.gov/19505082/)
67. G. E. Cragg, A. L. Efros, Suppression of auger processes in confined structures. *Nano Lett.* **10**, 313–317 (2010). doi: [10.1021/nl903592h](https://doi.org/10.1021/nl903592h); pmid: [20017564](https://pubmed.ncbi.nlm.nih.gov/20017564/)
68. W. K. Bae *et al.*, Controlled alloying of the core-shell interface in CdSe/Cd quantum dots for suppression of Auger recombination. *ACS Nano* **7**, 3411–3419 (2013). doi: [10.1021/nn4002825](https://doi.org/10.1021/nn4002825); pmid: [23521208](https://pubmed.ncbi.nlm.nih.gov/23521208/)
69. F. Fan *et al.*, Continuous-wave lasing in colloidal quantum dot solids enabled by facet-selective epitaxy. *Nature* **544**, 75–79 (2017). doi: [10.1038/nature21424](https://doi.org/10.1038/nature21424); pmid: [28321128](https://pubmed.ncbi.nlm.nih.gov/28321128/)
70. J. Roh, Y.-S. Park, J. Lim, V. I. Klimov, Optically pumped colloidal quantum-dot lasing in LED-like devices with an integrated optical cavity. *Nat. Commun.* **11**, 271 (2020). doi: [10.1038/s41467-019-14014-3](https://doi.org/10.1038/s41467-019-14014-3); pmid: [31937771](https://pubmed.ncbi.nlm.nih.gov/31937771/)
71. M. Grundmann, The present status of quantum dot lasers. *Phys. E* **5**, 167–184 (1999). doi: [10.1016/S1386-9477\(99\)00041-7](https://doi.org/10.1016/S1386-9477(99)00041-7)
72. K. Otsubo *et al.*, Temperature-insensitive eye-opening under 10-Gb/s modulation of 1.3-μm P-doped quantum-dot lasers without current adjustments. *Jpn. J. Appl. Phys.* **43** (No. 8B), L1124–L1126 (2004). doi: [10.1143/JJAP.43.L1124](https://doi.org/10.1143/JJAP.43.L1124)
73. T. Kageyama *et al.*, in 2011 Conference on Lasers and Electro-Optics Europe and 12th European Quantum Electronics Conference (CLEO EUROPE/EQEC) (IEEE, 2011); <http://ieeexplore.ieee.org/document/5943701>.
74. Y. Arakawa, T. Nakamura, J. Kwoon, Quantum dot lasers for silicon photonics. *Semicond. Semimet.* **101**, 91–138 (2019). doi: [10.1016/j.bssemsem.2019.07.007](https://doi.org/10.1016/j.bssemsem.2019.07.007)
75. H. Lim, S. Tsao, W. Zhang, M. Razeghi, High-performance InAs quantum-dot infrared photodetectors grown on InP substrate operating at room temperature. *Appl. Phys. Lett.* **90**, 131112 (2007). doi: [10.1063/1.2719160](https://doi.org/10.1063/1.2719160)
76. P. Martyniuk, A. Rogalski, Quantum-dot infrared photodetectors: Status and outlook. *Prog. Quantum Electron.* **32**, 89–120 (2008). doi: [10.1016/j.pquantelec.2008.07.001](https://doi.org/10.1016/j.pquantelec.2008.07.001)
77. B. Chen *et al.*, Low dark current high gain InAs quantum dot avalanche photodiodes monolithically grown on Si. *ACS Photonics* **7**, 528–533 (2020). doi: [10.1021/acsphotons.9b01709](https://doi.org/10.1021/acsphotons.9b01709)
78. A. Ren, L. Yuan, H. Xu, J. Wu, Z. Wang, Recent progress of III–V quantum dot infrared photodetectors on silicon. *J. Mater. Chem. C Mater. Opt. Electron. Devices* **7**, 14441–14453 (2019). doi: [10.1039/C9TC0573B](https://doi.org/10.1039/C9TC0573B)
79. R. Saran, R. J. Curry, Lead sulphide nanocrystal photodetector technologies. *Nat. Photonics* **10**, 81–92 (2016). doi: [10.1038/nphoton.2015.280](https://doi.org/10.1038/nphoton.2015.280)
80. G. Konstantatos *et al.*, Ultrasensitive solution-cast quantum dot photodetectors. *Nature* **442**, 180–183 (2006). doi: [10.1038/nature04855](https://doi.org/10.1038/nature04855); pmid: [16838017](https://pubmed.ncbi.nlm.nih.gov/16838017/)
81. J. P. Clifford *et al.*, Fast, sensitive and spectrally tuneable colloidal quantum-dot photodetectors. *Nat. Nanotechnol.* **4**, 40–44 (2009). doi: [10.1038/nano.2008.133](https://doi.org/10.1038/nano.2008.133); pmid: [19119213](https://pubmed.ncbi.nlm.nih.gov/19119213/)
82. C. Livache, B. Martinez, N. Goubert, J. Ramade, E. Lhuillier, Road map for nanocrystal based infrared photodetectors. *Front. Chem.* **6**, 575 (2018). doi: [10.3389/fchem.2018.00575](https://doi.org/10.3389/fchem.2018.00575); pmid: [30547026](https://pubmed.ncbi.nlm.nih.gov/30547026/)
83. M. M. Ackerman, X. Tang, P. Guyot-Sionnest, Fast and sensitive colloidal quantum dot mid-wave infrared photodetectors. *ACS Nano* **12**, 7264–7271 (2018). doi: [10.1021/acsnano.8b03425](https://doi.org/10.1021/acsnano.8b03425); pmid: [29975502](https://pubmed.ncbi.nlm.nih.gov/29975502/)
84. S. Keuleyan, E. Lhuillier, V. Brajuskovic, P. Guyot-Sionnest, Mid-infrared HgTe colloidal quantum dot photodetectors. *Nat. Photonics* **5**, 489–493 (2011). doi: [10.1038/nphoton.2011.142](https://doi.org/10.1038/nphoton.2011.142)
85. X. Tang, M. M. Ackerman, M. Chen, P. Guyot-Sionnest, Dual-band infrared imaging using stacked colloidal quantum dot photodiodes. *Nat. Photonics* **13**, 277–282 (2019). doi: [10.1038/s41566-019-0362-1](https://doi.org/10.1038/s41566-019-0362-1)
86. Z. Deng, K. S. Jeong, P. Guyot-Sionnest, Colloidal quantum dots intraband photodetectors. *ACS Nano* **8**, 11707–11714 (2014). doi: [10.1021/nn505092a](https://doi.org/10.1021/nn505092a); pmid: [25343383](https://pubmed.ncbi.nlm.nih.gov/25343383/)
87. J. Kim, D. Choi, K. S. Jeong, Self-doped colloidal semiconductor nanocrystals with intraband transitions in steady state. *Chem. Commun.* **54**, 8435–8445 (2018). doi: [10.1039/C8CC02488J](https://doi.org/10.1039/C8CC02488J); pmid: [2972153](https://pubmed.ncbi.nlm.nih.gov/2972153/)
88. I. Ramiro *et al.*, Mid- and long-wave infrared optoelectronics via intraband transitions in PbS colloidal quantum dots. *Nano Lett.* **20**, 1003–1008 (2020). doi: [10.1021/acs.nanolett.9b04130](https://doi.org/10.1021/acs.nanolett.9b04130); pmid: [31934762](https://pubmed.ncbi.nlm.nih.gov/31934762/)
89. C. Livache *et al.*, A colloidal quantum dot infrared photodetector and its use for intraband detection. *Nat. Commun.* **10**, 2125 (2019). doi: [10.1038/s41467-019-10170-8](https://doi.org/10.1038/s41467-019-10170-8); pmid: [31073132](https://pubmed.ncbi.nlm.nih.gov/31073132/)
90. G. Konstantatos *et al.*, Hybrid graphene-quantum dot phototransistors with ultrahigh gain. *Nat. Nanotechnol.* **7**, 363–368 (2012). doi: [10.1038/nnano.2012.60](https://doi.org/10.1038/nnano.2012.60); pmid: [22562036](https://pubmed.ncbi.nlm.nih.gov/22562036/)
91. F. P. García de Arquer *et al.*, Field-emission from quantum-dot-in-perovskite solids. *Nat. Commun.* **8**, 14757 (2017). doi: [10.1038/ncomms14757](https://doi.org/10.1038/ncomms14757); pmid: [28337981](https://pubmed.ncbi.nlm.nih.gov/28337981/)
92. D. Kufer, G. Konstantatos, Photo-FETs: Phototransistors enabled by 2D and 0D nanomaterials. *ACS Photonics* **3**, 2197–2210 (2016). doi: [10.1021/acspophotonics.6b00391](https://doi.org/10.1021/acspophotonics.6b00391)
93. F. P. García de Arquer, A. Armin, P. Meredith, E. H. Sargent, Solution-processed semiconductors for next-generation photodetectors. *Nat. Rev. Mater.* **2**, 16100 (2017). doi: [10.1038/natrevmats.2016.100](https://doi.org/10.1038/natrevmats.2016.100)
94. G. Konstantatos, Current status and technological prospect of photodetectors based on two-dimensional materials. *Nat. Commun.* **9**, 5266 (2018). doi: [10.1038/s41467-018-07643-7](https://doi.org/10.1038/s41467-018-07643-7); pmid: [30531824](https://pubmed.ncbi.nlm.nih.gov/30531824/)
95. S. Goossens *et al.*, Broadband image sensor array based on graphene-CMOS integration. *Nat. Photonics* **11**, 366–371 (2017). doi: [10.1038/nphoton.2017.75](https://doi.org/10.1038/nphoton.2017.75)
96. V. Adinolfi, E. H. Sargent, Photovoltaic field-effect transistors. *Nature* **542**, 324–327 (2017). doi: [10.1038/nature21050](https://doi.org/10.1038/nature21050); pmid: [28178236](https://pubmed.ncbi.nlm.nih.gov/28178236/)
97. D. Y. Kim *et al.*, PbSe nanocrystal-based infrared-to-visible up-conversion device. *Nano Lett.* **11**, 2109–2113 (2011). doi: [10.1021/nl0020704h](https://doi.org/10.1021/nl0020704h); pmid: [21504192](https://pubmed.ncbi.nlm.nih.gov/21504192/)
98. W. Zhou *et al.*, Solution-processed upconversion photodetectors based on quantum dots. *Nat. Electron.* **3**, 251–258 (2020). doi: [10.1038/s41928-020-0388-x](https://doi.org/10.1038/s41928-020-0388-x)
99. Q. Chen *et al.*, All-inorganic perovskite nanocrystal scintillators. *Nature* **561**, 88–93 (2018). doi: [10.1038/s41586-018-0451-1](https://doi.org/10.1038/s41586-018-0451-1); pmid: [30150772](https://pubmed.ncbi.nlm.nih.gov/30150772/)
100. J. Bao, M. G. Bawendi, A colloidal quantum dot spectrometer. *Nature* **523**, 67–70 (2015). doi: [10.1038/nature14576](https://doi.org/10.1038/nature14576); pmid: [26135449](https://pubmed.ncbi.nlm.nih.gov/26135449/)
101. S. A. McDonald *et al.*, Solution-processed PbS quantum dot infrared photodetectors and photovoltaics. *Nat. Mater.* **4**, 138–142 (2005). doi: [10.1038/nmat1299](https://doi.org/10.1038/nmat1299); pmid: [16540806](https://pubmed.ncbi.nlm.nih.gov/16540806/)
102. I. Gur, N. A. Fromer, M. L. Geier, A. P. Alivisatos, Air-stable all-inorganic nanocrystal solar cells processed from solution. *Science* **310**, 462–465 (2005). doi: [10.1126/science.1117908](https://doi.org/10.1126/science.1117908); pmid: [16239470](https://pubmed.ncbi.nlm.nih.gov/16239470/)
103. A. R. Kirmani, J. M. Luther, M. Abolhasani, A. Amassian, Colloidal quantum dot photovoltaics: Current progress and path to gigawatt scale enabled by smart manufacturing. *ACS Energy Lett.* **5**, 3069–3100 (2020). doi: [10.1021/acsenergylett.0c01453](https://doi.org/10.1021/acsenergylett.0c01453)
104. S. Pradhan, A. Stavrinidis, S. Gupta, S. Christodoulou, G. Konstantatos, Breaking the open-circuit voltage deficit floor in PbS quantum dot solar cells through synergistic ligand and architecture engineering. *ACS Energy Lett.* **2**, 1444–1449 (2017). doi: [10.1021/acsenergylett.7b00244](https://doi.org/10.1021/acsenergylett.7b00244)
105. C.-H. M. Chuang *et al.*, Open-circuit voltage deficit, radiative sub-bandgap states, and prospects in quantum dot solar cells. *Nano Lett.* **15**, 3286–3294 (2015). doi: [10.1021/acs.nanolett.5b00513](https://doi.org/10.1021/acs.nanolett.5b00513); pmid: [25927871](https://pubmed.ncbi.nlm.nih.gov/25927871/)
106. S. Kahmann, M. A. Loi, Trap states in lead chalcogenide colloidal quantum dots - Origin, impact, and remedies. *Appl. Phys. Rev.* **7**, 041305 (2020). doi: [10.1063/5.0019800](https://doi.org/10.1063/5.0019800)
107. C.-H. M. Chuang, P. R. Brown, V. Bulović, M. G. Bawendi, Improved performance and stability in quantum dot solar cells through band alignment engineering. *Nat. Mater.* **13**, 796–801 (2014). doi: [10.1038/nmat3984](https://doi.org/10.1038/nmat3984); pmid: [24859641](https://pubmed.ncbi.nlm.nih.gov/24859641/)
108. T. Kim, X. Jin, J. H. Song, S. Jeong, T. Park, Efficiency limit of colloidal quantum dot solar cells: Effect of optical interference on active layer absorption. *ACS Energy Lett.* **5**, 248–251 (2020). doi: [10.1021/acsenergylett.9b02504](https://doi.org/10.1021/acsenergylett.9b02504)
109. A. K. Rath *et al.*, Solution-processed inorganic bulk nano-heterojunctions and their application to solar cells. *Nat. Photonics* **6**, 529–534 (2012). doi: [10.1038/nphoton.2012.139](https://doi.org/10.1038/nphoton.2012.139)
110. M. Liu *et al.*, Hybrid organic-inorganic inks flatten the energy landscape in colloidal quantum dot solids. *Nat. Mater.* **16**, 258–263 (2017). doi: [10.1038/nmat4800](https://doi.org/10.1038/nmat4800); pmid: [27842072](https://pubmed.ncbi.nlm.nih.gov/27842072/)

111. B. Sun *et al.*, Monolayer perovskite bridges enable strong quantum dot coupling for efficient solar cells. *Joule* **4**, 1542–1556 (2020). doi: [10.1016/j.joule.2020.05.011](https://doi.org/10.1016/j.joule.2020.05.011)
112. S.-W. Baek *et al.*, Efficient hybrid colloidal quantum dot/organic solar cells mediated by near-infrared sensitizing small molecules. *Nat. Energy* **4**, 969–976 (2019). doi: [10.1038/s41560-019-0492-1](https://doi.org/10.1038/s41560-019-0492-1)
113. A. Swarnkar *et al.*, Quantum dot-induced phase stabilization of α -CsPbI₃ perovskite for high-efficiency photovoltaics. *Science* **354**, 92–95 (2016). doi: [10.1126/science.aag2700](https://doi.org/10.1126/science.aag2700); pmid: [27846497](#)
114. M. Hao *et al.*, Ligand-assisted cation-exchange engineering for high-efficiency colloidal Cs_{1-x}Pb_xI₃ quantum dot solar cells with reduced phase segregation. *Nat. Energy* **5**, 79–88 (2020). doi: [10.1038/s41560-019-0535-7](https://doi.org/10.1038/s41560-019-0535-7)
115. J. Yuan *et al.*, Metal halide perovskites in quantum dot solar cells: Progress and prospects. *Joule* **4**, 1160–1185 (2020). doi: [10.1016/j.joule.2020.04.006](https://doi.org/10.1016/j.joule.2020.04.006)
116. B. Chen *et al.*, Enhanced optical path and electron diffusion length enable high-efficiency perovskite tandems. *Nat. Commun.* **11**, 1257 (2020). doi: [10.1038/s41467-020-15077-3](https://doi.org/10.1038/s41467-020-15077-3); pmid: [32152324](#)
117. M. J. Crane, D. M. Krupa, D. R. Gamelin, Detailed-balance analysis of Yb³⁺:CsPb(Cl_{1-x}Br_x)₃ quantum-cutting layers for high-efficiency photovoltaics under real-world conditions. *Energy Environ. Sci.* **12**, 2486–2495 (2019). doi: [10.1039/C9EE01493D](https://doi.org/10.1039/C9EE01493D)
118. W. H. Weber, J. Lambe, Luminescent greenhouse collector for solar radiation. *Appl. Opt.* **15**, 2299–2300 (1976). doi: [10.1364/AO.15.002299](https://doi.org/10.1364/AO.15.002299); pmid: [20165383](#)
119. M. G. Debije, P. P. C. Verbunt, Thirty years of luminescent solar concentrator research: Solar energy for the built environment. *Adv. Energy Mater.* **2**, 12–35 (2012). doi: [10.1002/aenm.201100554](https://doi.org/10.1002/aenm.201100554)
120. H.-J. Song *et al.*, Performance limits of luminescent solar concentrators tested with seed/quantum-well quantum dots in a selective-reflector-based optical cavity. *Nano Lett.* **18**, 395–404 (2018). doi: [10.1021/acs.nanolett.7b04263](https://doi.org/10.1021/acs.nanolett.7b04263); pmid: [29226688](#)
121. F. Meinardi *et al.*, Large-area luminescent solar concentrators based on ‘Stokes-shift-engineered’ nanocrystals in a mass-polymerized PMMA matrix. *Nat. Photonics* **8**, 392–399 (2014). doi: [10.1038/nphoton.2014.54](https://doi.org/10.1038/nphoton.2014.54)
122. N. D. Bronstein *et al.*, Quantum dot luminescent concentrator cavity exhibiting 30-fold concentration. *ACS Photonics* **2**, 1576–1583 (2015). doi: [10.1021/acspolymers.5b00334](https://doi.org/10.1021/acspolymers.5b00334)
123. F. Meinardi *et al.*, Highly efficient large-area colourless luminescent solar concentrators using heavy-metal-free colloidal quantum dots. *Nat. Nanotechnol.* **10**, 878–885 (2015). doi: [10.1038/nnano.2015.178](https://doi.org/10.1038/nnano.2015.178); pmid: [26301902](#)
124. M. R. Bergren *et al.*, High-performance CuInS₂ quantum dot laminated glass luminescent solar concentrators for windows. *ACS Energy Lett.* **3**, 520–525 (2018). doi: [10.1021/acsenergylett.7b01346](https://doi.org/10.1021/acsenergylett.7b01346)
125. A. S. Fuhr *et al.*, Light emission mechanisms in CuInS₂ quantum dots evaluated by spectral electrochemistry. *ACS Photonics* **4**, 2425–2435 (2017). doi: [10.1021/acspolymers.7b00560](https://doi.org/10.1021/acspolymers.7b00560)
126. K. Wu, H. Li, V. I. Klimov, Tandem luminescent solar concentrators based on engineered quantum dots. *Nat. Photonics* **12**, 105–110 (2018). doi: [10.1038/s41566-017-0070-7](https://doi.org/10.1038/s41566-017-0070-7)
127. N. S. Makarov *et al.*, Fiber-coupled luminescent concentrators for medical diagnostics, agriculture, and telecommunications. *ACS Nano* **13**, 9112–9121 (2019). doi: [10.1021/acsnano.9b03335](https://doi.org/10.1021/acsnano.9b03335); pmid: [31291097](#)
128. L. Trahey *et al.*, Energy storage emerging: A perspective from the Joint Center for Energy Storage Research. *Proc. Natl. Acad. Sci. U.S.A.* **117**, 12550–12557 (2020). doi: [10.1073/pnas.1821672117](https://doi.org/10.1073/pnas.1821672117); pmid: [32513633](#)
129. X.-B. Li, C.-H. Tung, L.-Z. Wu, Semiconducting quantum dots for artificial photosynthesis. *Nat. Rev. Chem.* **2**, 160–173 (2018). doi: [10.1038/s41570-018-0024-8](https://doi.org/10.1038/s41570-018-0024-8)
130. J. Wang *et al.*, Enabling visible-light-driven selective CO₂ reduction by doping quantum dots: Trapping electrons and suppressing H₂ evolution. *Angew. Chem. Int. Ed.* **57**, 16447–16451 (2018). doi: [10.1002/anie.201810550](https://doi.org/10.1002/anie.201810550); pmid: [30350910](#)
131. E. A. Weiss, Designing the surfaces of semiconductor quantum dots for colloidal photocatalysis. *ACS Energy Lett.* **2**, 1005–1013 (2017). doi: [10.1021/acsenergylett.7b00061](https://doi.org/10.1021/acsenergylett.7b00061)
132. S. W. Boettcher, T. E. Mallouk, F. E. Osterloh, Themed issue on water splitting and photocatalysis. *J. Mater. Chem. A* **Mater. Energy Sustain.** **4**, 2764–2765 (2016). doi: [10.1039/C6TA90014C](https://doi.org/10.1039/C6TA90014C)
133. H. Wu, X. Li, C. Tung, L. Wu, Semiconductor quantum dots: An emerging candidate for CO₂ photoreduction. *Adv. Mater.* **31**, 1900709 (2019). doi: [10.1002/adma.201900709](https://doi.org/10.1002/adma.201900709)
134. D. W. Wakerley *et al.*, Solar-driven reforming of lignocellulose to H₂ with a CdS/CdO_x photocatalyst. *Nat. Energy* **2**, 17021 (2017). doi: [10.1038/nenergy.2017.21](https://doi.org/10.1038/nenergy.2017.21)
135. T. Uekert, M. F. Kuehnel, D. W. Wakerley, E. Reisner, Plastic waste as a feedstock for solar-driven H₂ generation. *Energy Environ. Sci.* **11**, 2853–2857 (2018). doi: [10.1039/C8EE01408F](https://doi.org/10.1039/C8EE01408F)
136. X. Chen, N. Li, Z. Kong, W.-J. Ong, X. Zhao, Photocatalytic fixation of nitrogen to ammonia: State-of-the-art advancements and future prospects. *Mater. Horiz.* **5**, 9–27 (2018). doi: [10.1039/C7MH00557A](https://doi.org/10.1039/C7MH00557A)
137. U. A. Rani, L. Y. Ng, Y. C. Ng, E. Mahmoudi, A review of carbon quantum dots and their applications in wastewater treatment. *Adv. Colloid Interface Sci.* **278**, 102124 (2020). doi: [10.1016/j.jcis.2020.102124](https://doi.org/10.1016/j.jcis.2020.102124); pmid: [32142942](#)
138. K. K. Sakimoto, A. B. Wong, P. Yang, Self-photosensitization of nonphotosynthetic bacteria for solar-to-chemical production. *Science* **351**, 74–77 (2016). doi: [10.1126/science.aad3317](https://doi.org/10.1126/science.aad3317); pmid: [26721997](#)
139. H. Luo, Q. Guo, P. Á. Szilágyi, A. B. Jorge, M. M. Titirici, Carbon dots in solar-to-hydrogen conversion. *Trends Chem.* **2**, 623–637 (2020). doi: [10.1016/j.trechm.2020.04.007](https://doi.org/10.1016/j.trechm.2020.04.007)
140. H. Jung *et al.*, Highly efficient and stable CO₂ reduction photocatalyst with a hierarchical structure of mesoporous TiO₂ on 3D graphene with few-layered MoS₂. *ACS Sustain. Chem. & Eng.* **6**, 5718–5724 (2018). doi: [10.1021/acssuschemeng.8b00002](https://doi.org/10.1021/acssuschemeng.8b00002)
141. T. Takata, K. Domen, Particulate photocatalysts for water splitting: Recent advances and future prospects. *ACS Energy Lett.* **4**, 542–549 (2019). doi: [10.1021/acsenergylett.8b02209](https://doi.org/10.1021/acsenergylett.8b02209)
142. C. Anton, K. S. Ranade, Eds., *Quantum Technology, From Research to Application* (National Academy of Science and Engineering, 2015); <https://en.acatech.de/publication/perspektiven-der-quantentechnologien>.
143. P. Borri *et al.*, Ultralow dephasing time in InGaAs quantum dots. *Phys. Rev. Lett.* **87**, 157401 (2001). doi: [10.1103/PhysRevLett.87.157401](https://doi.org/10.1103/PhysRevLett.87.157401); pmid: [11580725](#)
144. T. H. Stievater *et al.*, Rabi oscillations of excitons in single quantum dots. *Phys. Rev. Lett.* **87**, 133603 (2001). doi: [10.1103/PhysRevLett.87.133603](https://doi.org/10.1103/PhysRevLett.87.133603); pmid: [11580588](#)
145. A. Greilich *et al.*, Mode locking of electron spin coherences in singly charged quantum dots. *Science* **313**, 341–345 (2006). doi: [10.1126/science.1128215](https://doi.org/10.1126/science.1128215); pmid: [16857937](#)
146. J. R. Petta *et al.*, Coherent manipulation of coupled electron spins in semiconductor quantum dots. *Science* **309**, 2180–2184 (2005). doi: [10.1126/science.1116955](https://doi.org/10.1126/science.1116955); pmid: [16141370](#)
147. D. Brunner *et al.*, A coherent single-hole spin in a semiconductor. *Science* **325**, 70–72 (2009). doi: [10.1126/science.1173684](https://doi.org/10.1126/science.1173684); pmid: [19574387](#)
148. K. De Greve *et al.*, Ultrafast coherent control and suppressed nuclear feedback of a single quantum dot hole qubit. *Nat. Phys.* **7**, 872–878 (2011). doi: [10.1038/nphys2078](https://doi.org/10.1038/nphys2078)
149. P. Michler, *Quantum Dots for Quantum Information Technologies* (Springer, 2017).
150. P. Michler *et al.*, A quantum dot single-photon turnstile device. *Science* **290**, 2282–2285 (2000). doi: [10.1126/science.290.5500.2282](https://doi.org/10.1126/science.290.5500.2282); pmid: [11125136](#)
151. N. Somaschi *et al.*, Near-optimal single-photon sources in the solid state. *Nat. Photonics* **10**, 340–345 (2016). doi: [10.1038/nphoton.2016.23](https://doi.org/10.1038/nphoton.2016.23)
152. S. Unsleber *et al.*, Highly indistinguishable on-demand resonance fluorescence photons from a deterministic quantum dot micropillar device with 74% extraction efficiency. *Opt. Express* **24**, 8539–8546 (2016). doi: [10.1364/OE.24.008539](https://doi.org/10.1364/OE.24.008539); pmid: [27137291](#)
153. L. Schweikert *et al.*, On-demand generation of background-free single photons from a solid-state source. *Appl. Phys. Lett.* **112**, 093106 (2018). doi: [10.1063/1.5020038](https://doi.org/10.1063/1.5020038)
154. O. Gazzano *et al.*, Bright solid-state sources of indistinguishable single photons. *Nat. Commun.* **4**, 1425 (2013). doi: [10.1038/ncomms2434](https://doi.org/10.1038/ncomms2434); pmid: [23385570](#)
155. H. Utzat *et al.*, Coherent single-photon emission from colloidal lead halide perovskite quantum dots. *Science* **363**, 1068–1072 (2019). doi: [10.1126/science.aau7392](https://doi.org/10.1126/science.aau7392); pmid: [30792359](#)
156. X. Lin *et al.*, Electrically-driven single-photon sources based on colloidal quantum dots with near-optimal antibunching at room temperature. *Nat. Commun.* **8**, 1132 (2017). doi: [10.1038/s41467-017-01379-6](https://doi.org/10.1038/s41467-017-01379-6); pmid: [29070867](#)
157. M. J. Holmes, S. Kako, K. Choi, M. Arita, Y. Arakawa, Single photons from a hot solid-state emitter at 350 K. *ACS Photonics* **3**, 543–546 (2016). doi: [10.1021/acspolymers.6b00112](https://doi.org/10.1021/acspolymers.6b00112)
158. C. Santori, D. Fattal, J. Vucković, G. S. Solomon, Y. Yamamoto, Indistinguishable photons from a single-photon device. *Nature* **419**, 594–597 (2002). doi: [10.1038/nature01086](https://doi.org/10.1038/nature01086); pmid: [12374958](#)
159. K. Toyoda, R. Hiji, A. Noguchi, S. Urabe, Hong-Ou-Mandel interference of two photons in trapped ions. *Nature* **527**, 74–77 (2015). doi: [10.1038/nature15735](https://doi.org/10.1038/nature15735); pmid: [26536958](#)
160. X. Ding *et al.*, On-demand single photons with high extraction efficiency and near-unity indistinguishability from a resonantly driven quantum dot in a micropillar. *Phys. Rev. Lett.* **116**, 020401 (2016). doi: [10.1103/PhysRevLett.116.020401](https://doi.org/10.1103/PhysRevLett.116.020401); pmid: [26824530](#)
161. O. Benson, C. Santori, M. Pelton, Y. Yamamoto, Regulated and entangled photons from a single quantum dot. *Phys. Rev. Lett.* **84**, 2513–2516 (2000). doi: [10.1103/PhysRevLett.84.2513](https://doi.org/10.1103/PhysRevLett.84.2513); pmid: [1018923](#)
162. N. Akopian *et al.*, Entangled photon pairs from semiconductor quantum dots. *Phys. Rev. Lett.* **95**, 130501 (2006). doi: [10.1103/PhysRevLett.95.130501](https://doi.org/10.1103/PhysRevLett.95.130501); pmid: [16711973](#)
163. R. J. Young *et al.*, Improved fidelity of triggered entangled photons from single quantum dots. *New J. Phys.* **8**, 29–29 (2006). doi: [10.1088/1367-2630/8/2/029](https://doi.org/10.1088/1367-2630/8/2/029)
164. M. Müller, S. Bounouar, K. D. Jöns, M. Glässl, P. Michler, On-demand generation of indistinguishable polarization-entangled photon pairs. *Nat. Photonics* **8**, 224–228 (2014). doi: [10.1038/nphoton.2013.377](https://doi.org/10.1038/nphoton.2013.377)
165. D. Huber *et al.*, Strain-tunable GaAs quantum dot: A nearly dephasing-free source of entangled photon pairs on demand. *Phys. Rev. Lett.* **121**, 033902 (2018). doi: [10.1103/PhysRevLett.121.033902](https://doi.org/10.1103/PhysRevLett.121.033902); pmid: [30085806](#)
166. M. Müller *et al.*, Quantum-dot single-photon sources for entanglement enhanced interferometry. *Phys. Rev. Lett.* **118**, 257402 (2017). doi: [10.1103/PhysRevLett.118.257402](https://doi.org/10.1103/PhysRevLett.118.257402); pmid: [28696738](#)
167. I. Schwartz *et al.*, Deterministic generation of a cluster state of entangled photons. *Science* **354**, 434–437 (2016). doi: [10.1126/science.ah4758](https://doi.org/10.1126/science.ah4758); pmid: [27608669](#)
168. P. Michler *et al.*, Quantum correlation among photons from a single quantum dot at room temperature. *Nature* **406**, 968–970 (2000). doi: [10.1038/35023100](https://doi.org/10.1038/35023100); pmid: [10984045](#)
169. G. Rainò *et al.*, Superfluorescence from lead halide perovskite quantum dot superlattices. *Nature* **563**, 671–675 (2018). doi: [10.1038/s41586-018-0683-0](https://doi.org/10.1038/s41586-018-0683-0); pmid: [30405237](#)
170. M. P. Hendricks, M. P. Campos, G. T. Cleveland, I. Jen-La Plante, J. S. Owen, A tunable library of substituted thiourea precursors to metal sulfide nanocrystals. *Science* **348**, 1226–1230 (2015). doi: [10.1126/science.aaa2951](https://doi.org/10.1126/science.aaa2951); pmid: [26068846](#)
171. J. Jean *et al.*, Synthesis cost dictates the commercial viability of lead sulfide and perovskite quantum dot photovoltaics. *Energy Environ. Sci.* **11**, 2295–2305 (2018). doi: [10.1039/C8EE01348A](https://doi.org/10.1039/C8EE01348A)
172. Y. Pu, F. Cai, D. Wang, J.-X. Wang, J.-F. Chen, Colloidal synthesis of semiconductor quantum dots toward large-scale production: A review. *Ind. Eng. Chem. Res.* **57**, 1790–1802 (2018). doi: [10.1021/acs.iecr.7b04836](https://doi.org/10.1021/acs.iecr.7b04836)
173. O. Voznyi *et al.*, Machine learning accelerates discovery of optimal colloidal quantum dot synthesis. *ACS Nano* **13**, 11122–11128 (2019). doi: [10.1021/acsnano.9b03864](https://doi.org/10.1021/acsnano.9b03864); pmid: [31539477](#)
174. Y.-H. Won *et al.*, Highly efficient and stable InP/ZnSe/ZnS quantum dot light-emitting diodes. *Nature* **575**, 634–638 (2019). doi: [10.1038/s41586-019-171-5](https://doi.org/10.1038/s41586-019-171-5); pmid: [31776489](#)
175. J. Du, R. Singh, I. Fedin, A. S. Fuhr, V. I. Klimov, Spectroscopic insights into high defect tolerance of Zn:CuInSe₂ quantum-dot-sensitized solar cells. *Nat. Energy* **5**, 409–417 (2020). doi: [10.1038/s41560-020-0617-6](https://doi.org/10.1038/s41560-020-0617-6)
176. M. Berneche *et al.*, Solution-processed solar cells based on environmentally friendly AgBiS₂ nanocrystals. *Nat. Photonics* **10**, 521–525 (2016). doi: [10.1038/nphoton.2016.108](https://doi.org/10.1038/nphoton.2016.108)
177. D. P. Tabor *et al.*, Accelerating the discovery of materials for clean energy in the era of smart automation. *Nat. Rev. Mater.* **3**, 5–20 (2018). doi: [10.1038/s41578-018-0005-z](https://doi.org/10.1038/s41578-018-0005-z)
178. W. Walraven *et al.*, Setting carriers free: Healing faulty interfaces promotes delocalization and transport in nanocrystal solids. *ACS Nano* **13**, 12774–12786 (2019). doi: [10.1021/acsnano.9b04757](https://doi.org/10.1021/acsnano.9b04757); pmid: [31693334](#)
179. M. Liu *et al.*, Lattice anchoring stabilizes solution-processed semiconductors. *Nature* **570**, 96–101 (2019). doi: [10.1038/s41586-019-1239-7](https://doi.org/10.1038/s41586-019-1239-7); pmid: [3118515](#)

180. J. Yang, M. K. Choi, D.-H. Kim, T. Hyeon, Designed Assembly and Integration of Colloidal Nanocrystals for Device Applications. *Adv. Mater.* **28**, 1176–1207 (2016). doi: [10.1002/adma.201502851](https://doi.org/10.1002/adma.201502851); pmid: [26707709](https://pubmed.ncbi.nlm.nih.gov/26707709/)
181. Y. Wang, I. Fedin, H. Zhang, D. V. Talapin, Direct optical lithography of functional inorganic nanomaterials. *Science* **357**, 385–388 (2017). doi: [10.1126/science.aan2958](https://doi.org/10.1126/science.aan2958); pmid: [28751606](https://pubmed.ncbi.nlm.nih.gov/28751606/)
182. J. Yang *et al.*, Toward full-color electroluminescent quantum dot displays. *Nano Lett.* **21**, 26–33 (2021). doi: [10.1021/acs.nanolett.0c03939](https://doi.org/10.1021/acs.nanolett.0c03939); pmid: [33258610](https://pubmed.ncbi.nlm.nih.gov/33258610/)
183. V. I. Klimov *et al.*, Single-exciton optical gain in semiconductor nanocrystals. *Nature* **447**, 441–446 (2007). doi: [10.1038/nature05839](https://doi.org/10.1038/nature05839); pmid: [17522678](https://pubmed.ncbi.nlm.nih.gov/17522678/)
184. K. Wu, Y.-S. Park, J. Lim, V. I. Klimov, Towards zero-threshold optical gain using charged semiconductor quantum dots. *Nat. Nanotechnol.* **12**, 1140–1147 (2017). doi: [10.1038/nnano.2017.189](https://doi.org/10.1038/nnano.2017.189); pmid: [29035399](https://pubmed.ncbi.nlm.nih.gov/29035399/)
185. O. V. Kozlov *et al.*, Sub-single-exciton lasing using charged quantum dots coupled to a distributed feedback cavity. *Science* **365**, 672–675 (2019). doi: [10.1126/science.aax3489](https://doi.org/10.1126/science.aax3489); pmid: [31416959](https://pubmed.ncbi.nlm.nih.gov/31416959/)
186. C. Wang, L. Brian, Wehrenberg, Chui Y. Woo, Philippe Guyot-Sionnest, Light Emission and Amplification in Charged CdSe Quantum Dots (2004), doi:doi: [10.1021/JP0489830](https://doi.org/10.1021/JP0489830)
187. S. Yakunin *et al.*, Low-threshold amplified spontaneous emission and lasing from colloidal nanocrystals of caesium lead halide perovskites. *Nat. Commun.* **6**, 8056 (2015). doi: [10.1038/ncomms9056](https://doi.org/10.1038/ncomms9056); pmid: [26290056](https://pubmed.ncbi.nlm.nih.gov/26290056/)
188. C. She *et al.*, Red, yellow, green, and blue amplified spontaneous emission and lasing using colloidal CdSe nanoplatelets. *ACS Nano* **9**, 9475–9485 (2015). doi: [10.1021/acsnano.5b02509](https://doi.org/10.1021/acsnano.5b02509); pmid: [26302368](https://pubmed.ncbi.nlm.nih.gov/26302368/)
189. B. Guzelturk, M. Pelton, M. Olutas, H. V. Demir, Giant modal gain coefficients in colloidal II-VI nanoplatelets. *Nano Lett.* **19**, 277–282 (2019). doi: [10.1021/acs.nanolett.8b03891](https://doi.org/10.1021/acs.nanolett.8b03891); pmid: [30539638](https://pubmed.ncbi.nlm.nih.gov/30539638/)
190. S. Christodoulou *et al.*, Single-exciton gain and stimulated emission across the infrared telecom band from robust heavily doped PbS colloidal quantum dots. *Nano Lett.* **20**, 5909–5915 (2020). doi: [10.1021/acs.nanolett.0c01859](https://doi.org/10.1021/acs.nanolett.0c01859); pmid: [32662655](https://pubmed.ncbi.nlm.nih.gov/32662655/)
191. R. H. Gilmore *et al.*, Epitaxial dimers and auger-assisted detrapping in PbS quantum dot solids. *Matter* **1**, 250–265 (2019). doi: [10.1016/j.matt.2019.05.015](https://doi.org/10.1016/j.matt.2019.05.015)
192. M. Chen *et al.*, High carrier mobility in HgTe quantum dot solids improves mid-IR photodetectors. *ACS Photonics* **6**, 2358–2365 (2019). doi: [10.1021/acspophotonics.9b01050](https://doi.org/10.1021/acspophotonics.9b01050)
193. S. Zheng, J. Chen, E. M. J. Johansson, X. Zhang, PbS colloidal quantum dot inks for infrared solar cells. *iScience* **23**, 101753 (2020). doi: [10.1016/j.isci.2020.101753](https://doi.org/10.1016/j.isci.2020.101753); pmid: [33241199](https://pubmed.ncbi.nlm.nih.gov/33241199/)
194. R. D. Schaller, V. I. Klimov, High efficiency carrier multiplication in PbSe nanocrystals: Implications for solar energy conversion. *Phys. Rev. Lett.* **92**, 186601 (2004). doi: [10.1103/PhysRevLett.92.186601](https://doi.org/10.1103/PhysRevLett.92.186601); pmid: [15169518](https://pubmed.ncbi.nlm.nih.gov/15169518/)
195. M. V. Khenkin *et al.*, Consensus statement for stability assessment and reporting for perovskite photovoltaics based on ISOS procedures. *Nat. Energy* **5**, 35–49 (2020). doi: [10.1038/s41560-019-0529-5](https://doi.org/10.1038/s41560-019-0529-5)
196. A. Luque, A. Martí, C. Stanley, Understanding intermediate-band solar cells. *Nat. Photonics* **6**, 146–152 (2012). doi: [10.1038/nphoton.2012.1](https://doi.org/10.1038/nphoton.2012.1)
197. H. Li, K. Wu, J. Lim, H.-J. Song, V. I. Klimov, Doctor-blade deposition of quantum dots onto standard window glass for low-loss large-area luminescent solar concentrators. *Nat. Energy* **1**, 16157 (2016). doi: [10.1038/nenergy.2016.157](https://doi.org/10.1038/nenergy.2016.157)

ACKNOWLEDGMENTS

Funding: F.P.G.d.A. and E.H.S. acknowledge support from the Canada Research Chair. F.P.G.d.A. was also supported by the Ministry of Economy and Competitiveness of Spain through the “Severo Ochoa” program for Centres of Excellence in R&D (SEJ- 0522), Fundació Privada Cellex, Fundació Privada Mir-Puig, and the Generalitat de Catalunya through the CERCA program. D.V.T. was supported by the US Department of Defense (DOD) Air Force Office of Scientific Research under grant FA9550-18-1-0099 and MICCoM, as part of the Computational Materials Sciences Program funded by the US Department of Energy, Office of Science, Basic Energy Sciences, Materials Sciences and Engineering Division, through Argonne National Laboratory, under contract DE-AC02-06CH11357. V.I.K. acknowledges support from the Solar Photochemistry Program of the Chemical Sciences, Biosciences and Geosciences Division, Office of Basic Energy Sciences, Office of Science, US Department of Energy (overview of photophysical aspects of cQDs relevant to solar energy conversion) and the Laboratory Directed Research and Development program of Los Alamos National Laboratory under project 20200213DR (overview of studies of cQD lasers and LEDs). Y.A. acknowledges funding from JSPS KAKENHI Grant-in-Aid for Specially Promoted Research (15H05700). M.B. acknowledges the support from the Deutsche Forschungsgemeinschaft in the frame of the ICRC TRR 160 (projects A1 and B1) and by Mercur Foundation (grant Pe-2019-0022).

10.1126/science.aaz8541

Semiconductor quantum dots: Technological progress and future challenges

F. Pelayo García de Arquer, Dmitri V. Talapin, Victor I. Klimov, Yasuhiko Arakawa, Manfred Bayer, and Edward H. Sargent

Science, 373 (6555), eaaz8541.

DOI: 10.1126/science.aaz8541

Advances in colloidal quantum dots

The confinement found in colloidal semiconductor quantum dots enables the design of materials with tunable properties. García de Arquer *et al.* review the recent advances in methods for synthesis and surface functionalization of quantum dots that enable fine tuning of their optical, chemical, and electrical properties. These important developments have driven the commercialization of display and lighting applications and provide promising developments in the related fields of lasing and sensing. —MSL

View the article online

<https://www.science.org/doi/10.1126/science.aaz8541>

Permissions

<https://www.science.org/help/reprints-and-permissions>